An incubator with temperature gradient control

Carpaij, W.M.

Award date:
2006

TU/e technische universiteit eindhoven

Eindhoven University of Technology

Faculteit Technische Natuurkunde
Groep Transportfysica
Gebouw: Cascade
Postbus 513
5600 MB Eindhoven

Title: **An incubator with temperature gradient control**

Author: W.M.Carpaij

Reportnumber: R-1675-A

Date: August 2005

Group: Fluid Dynamics

Advisors: M.E.H. van Dongen
A.A. van Steenhoven
A.J.H. Frijns

I ABSTRACT

Over the recent years diagnostics in genetics are increasingly based on micro array technology as this technology is becoming considerably faster, more accurate and above all less expensive. In this line Organon Teknika, a former AKZO NOBEL BU, developed a '3D-MicroArray' technology using a porous (70%) Al-oxide substrate with 200 nm wide, through going, channels. Micro arrays deposited on these substrates reacted with patient samples in fractions of minutes instead of hours allowing for real time temperature intervention measurements. The conception, design and development of the special incubator realizing these intervention conditions, are the subject of this work.

To obtain relevant information from these hybridization reactions, sample temperatures of up to 75 °C have to be dealt with. Sample evaporation is then a major concern, all the more as direct sight on the 3D-MicroArray during hybridization has to be maintained. In order to address these problems the concept of a 'temperature gradient' incubator is defined and evaluated with model computations.

The technical design of the temperature gradient incubator comprises next to a resistive heater a Peltier device to generate this temperature gradient. A dynamic model, set up for this incubator system, helps to establish the optimal control for both this heater and Peltier device.

The characteristics and functioning of the temperature gradient incubator are observed in an experimental setup and used to evaluate its feasibility.

II SAMENVATTING

Genetica gerelateerde diagnostiek maakt in toenemende mate gebruik van microarray technologie sinds deze technologie aanzienlijk sneller, betrouwbaarder en vooral goedkoper is geworden. Zo ontwikkelde Organon Teknika, een voormalig AKZO NOBEL bedrijf, een '3D-MicroArray' technologie, waarin gebruik gemaakt wordt van een poreus (70%) Al-oxyde substraat bestaande uit, dwars door het materiaal lopende, 200nm brede kanaaltjes. Microarrays opgebracht op een dergelijk substraat reageren in onderdelen van minuten met patientenmonsters in plaats van in uren. Hierdoor zijn real-time temperatuur-interventie-metingen mogelijk. Concept, ontwerp en ontwikkeling van een speciale incubator voor de realisatie van deze interventie condities zijn het onderwerp van dit werk.

Om uit dergelijke hybridisatiereacties relevante informatie te verkrijgen zijn monstertemperaturen tot 75 °C nodig. Monsterverdamping is dan een groot probleem temeer omdat rechtstreeks zicht op de 3D-MicroArray ten alle tijden gewaarborgd moet blijven. Om deze problemen de baas te blijven is het concept van een 'temperatuur-gradient-incubator' gedefinieerd en geëvalueerd met behulp van model-berekeningen.

Het technische ontwerp van de temperatuur-gradient-incubator bevat naast een weerstands-verwarming ook nog een Peltier element voor de opwekking van deze temperatuur-gradient. Een dynamisch model voor dit incubator systeem is gebruikt voor de vaststelling van het optimale controle-algorithme voor zowel het verwarmings- als het Peltier-element.

De karakteristieken en het functioneren van de temperatuur-gradient-incubator zijn bestudeerd in een experimentele opstelling en op basis hiervan is de haalbaarheid van het systeem geëvalueerd.

Table of Contents

Report Section

Appendices

I THE FLOW-THROUGH MICROARRAY SYSTEM

1 Introduction

Between 1985 and 1990 two important inventions mark the developments in the field of biotechnology:

In 1985 Kary B. Mullis came up with the Polymerase Chain Reaction (PCR) technique (appendix I) while working as a chemist at the Cetus Corporation, a biotechnology firm in Emeryville, California, USA. With this technique, scientists were capable to generate millions of copies of a specific part of even a single DNA molecule which boosted research on and diagnosis of genetic phenomena. In recent years the technique is being applied to an ever increasing extent in forensic research because of its capability to link specific persons to minimal traces of human origin via DNA comparison.

In the late 1980s, Stephen P.A. Fodor and co-workers invented the micro array technology (appendix II). They combined and extended combinatorial chemistry and chip technology on a substrate of a few cm^2. This way they were able to obtain matrices (>100x100) of µm-sized cells with per cell specific, small (10-30 nucleotides long) s(ingle)s(tranded)DNA molecules inside. After incubation with a mixture of labeled ssDNA or ssRNA molecules (usually resulting from a PCR-like reaction) they proved that complementary sequences were bound to their counterparts in the concerning cell(s). Under a microscope these cells lighted up and, as their location could be related to the genetic code of the binding molecules on the spot, the originally unknown mixture of ssDNA or ssRNA molecules could be identified.

Further developments brought about new variants of the micro array technology, but these all shared a common drawback: incubation times in the range of hours. Therefore in the second half of the nineties Organon Teknika, a business unit of AKZO Nobel BV, active in diagnostic systems, decided to pursuit an own unique position in micro arrays. To get rid of these long incubation times without sacrificing any of the other specific features was defined as the most important research objective.

Already in the start of this project it was concluded that the main cause for prolonged incubation times in these micro arrays is their intrinsic flat structure and the fact that during this incubation the rather large DNA/RNA-fragments only by diffusion can reach their surface bounded counterparts. To minimize these effects a flow-through substrate was sought and found. The Anopore Al-oxide filter material (see Figure 1) appeared a promising candidate. This material has a precise, non-deformable honeycomb pore (diameter ca 200 nm) structure. It is an alumina matrix, electrochemically manufactured and of a very high purity. The material has also minimal auto fluorescence, is non-toxic and highly inert.

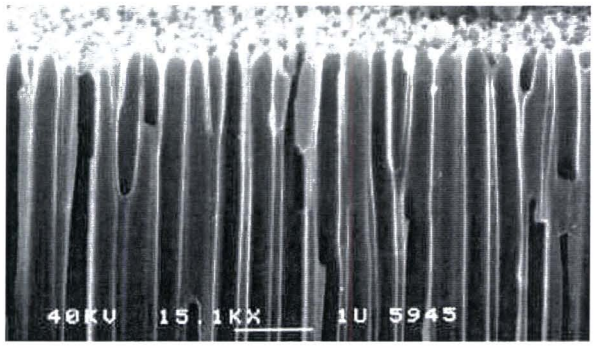

Figure 1
Anopore® Inorganic membrane of Al-oxide

With a porosity of the membrane of ca 70% this all results in a low flow resistance for water like fluids of 10-20 ml/(m^2.s.kPa).

2 The 3-Dimensional MicroArray

Just as on the glass of the microscope slide (appendix II), ssDNA fragments can be manipulated to bind endwise to the Al-oxide surface of the membrane. When dispensed in a droplet of ca 300 pl (Figure 2) containing one specific DNA fragment such a reagent will fill up a cylindrical domain inside the

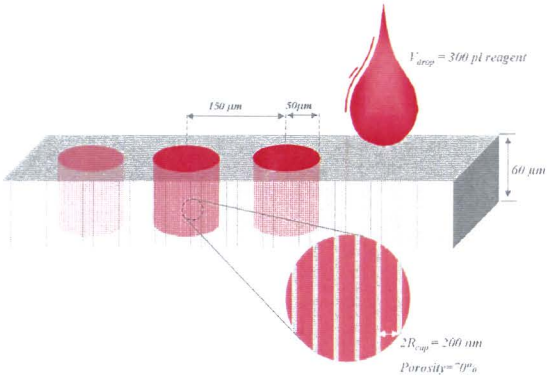

Figure 2
A 3D-MicroArray

membrane with a radius of 50 µm. This domain comprises a total number of about 1.6 million channels and opens up to the reagent an Al-oxide surface of ca 6 mm^2. The DNA fragments bind to the Al-oxide surface while the reagent evaporates leaving a spatially well defined micro array cell. As compared with the microscope slide micro array these cells have an over 500-fold larger binding surface.

Because the Al-oxide membrane is very brittle it is laminated between 2 plastic foils that have 4 corresponding holes leaving the membrane uncovered at those locations (Figure 3). These holes are 9 mm apart, have a diameter of 6mm and can accommodate a micro array of up to 2500 cells each.

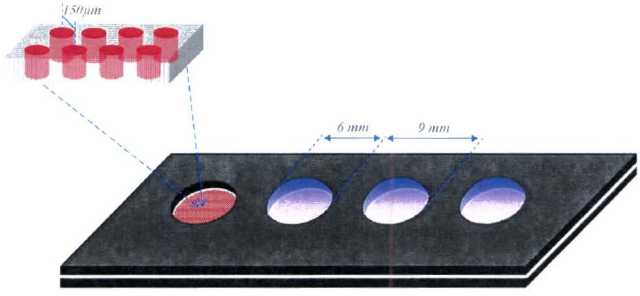

Figure 3
3D-MicroArray device with 4 arrays

The sample that has to react with 1 of the 4 micro arrays is deposited on the free membrane in the respective hole and covers it totally. Instead of circulating the sample fluid through the membrane via a closed flow circuit, an alternating air pressure is applied over the device which cycles the sample drop from above to underneath the membrane and vice versa. Because the membrane is so well defined and of a constant quality the resulting flow density is indeed very homogeneous and well adjustable.

First results (see Figure 4) supported the validity of the expectations that had arisen during the quest for

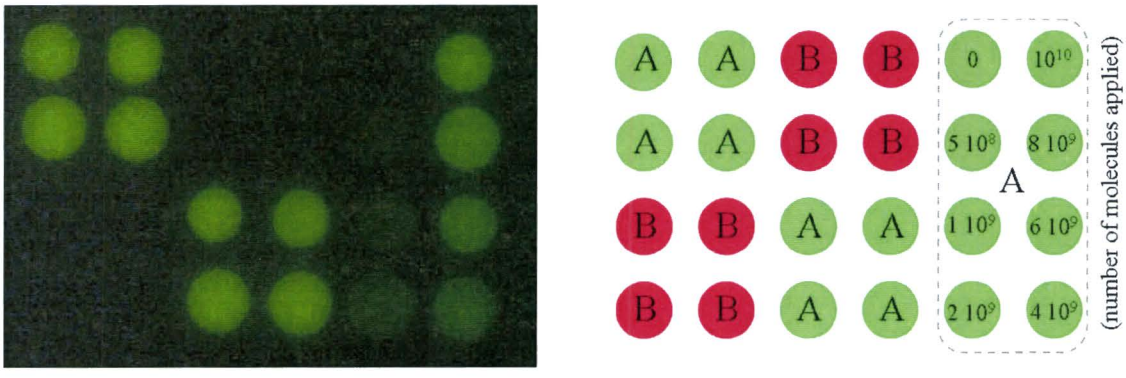

Figure 4[1]
First results with a 3D-MicroArray. A dose response experiment.

a 3D-MicroArray system and showed that within minutes relevant signals could be detected making real time intervention techniques possible. At the right of the figure the layout of the micro array is depicted. The cells in this array are spotted with oligo's (short DNA strands) of either sequence 'A' or 'B'. The 'A'

and 'B' sequence are completely different. For all the cells the same number of molecules has been used, except for the 2 columns at the right where a series of droplet with different concentrations has been applied as shown in the figure. The incubation of the micro array with a solution of DNA-strands complementary to 'A' and labeled with a fluorescent tag, gives the result as presented in the left part of the figure.

In Figure 5 a typical example of the dynamic behavior of different hybridization reactions is given. The top pictures show the end result, left a view of the fluorescence intensity at the end of incubation and at right, in red, this intensity as evaluated relatively. Also at right in black the number of nucleotide-mismatches in the DNA-oligo's used to coat each individual cell compared with the labeled (more or

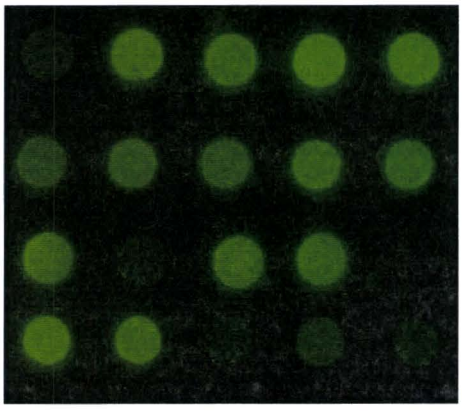

a)

C	1	2	0	2
8.4	54.6	49.0	63.2	59.4
2	2	2	2	2
30.5	42.6	37.4	48.4	46.2
1	4	3	3	7
49.0	4.6	50.6	48.8	0.0
1	3	5	3	C
56.2	53.6	5.2	14.2	8.3

b)

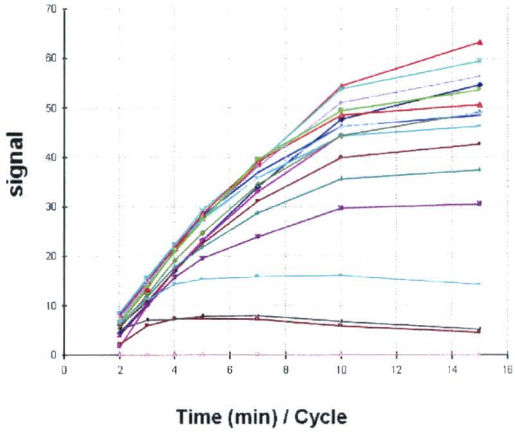

c)

Figure 5[1]
3D-MicroArray as dynamic measuring system.

a) Picture of fluorescent intensity after 15 cycles.

b) Relative fluorescent intensity in combination with # of nucleotide mismatches (c=control)

c) Reaction curves per cell.

less) complementary DNA-strands in solution that react with them. The 2 cells labeled C are used for control purposes.

The bottom left graph shows the binding curve for each individual cell. These real time binding curves

allow for reaction rate analysis and as reaction rate is related to the hybridization energy that in turn depends on the degree of complementarity, even sequencing is possible.

The feasibility of the 3D-MicroArray to perform real time measurements also allows for the observation of changes in hybridization under varying temperature settings. This is especially informative as melting temperatures for d(ouble)s(tranded)DNA fragments change considerably when the strands are not fully complementary but contain even a single mismatch (see Figure 6a). This phenomenon indeed shows up in the binding curves acquired for individual cells of the 3D-MicroArray when observed real time under temperature intervention (Figure 6b). So sequencing procedures will most probably gain by letting the reaction temperature dynamically vary over a trajectory just beyond the melting temperature of the fully complementary hybrid under investigation.

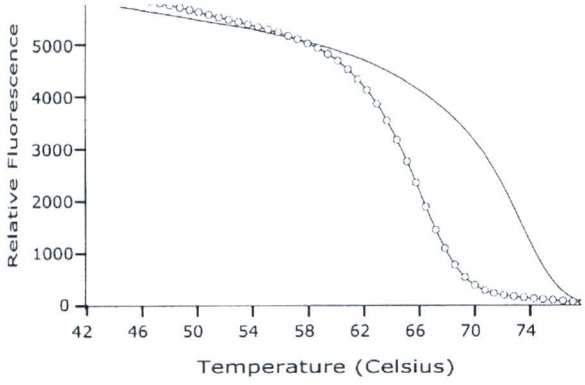

a) adapted from [2]
Melting curves for 2 dsDNA fragments,
(- - - complete match, - O- single mismatch)

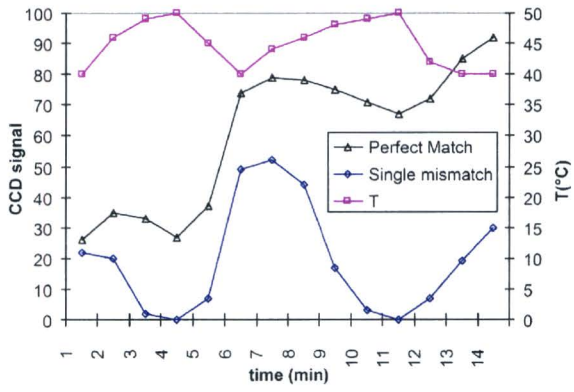

b) adapted from [1]
Temperature intervention hybridization

Figure 6
Hybridization Temperature Dependancy

It is clear that the 3D-MicroArray presents an exceptional variety of ways of application that only will show to full advantage in a well defined measuring system.

3 Problem Statement

The system based on the concept of the 3D-MicroArray as it is described above, will have to take into consideration its specific characteristics. Such a system is depicted in Figure 7 on the left and shows the four main functions relevant when performing a sample analysis.

1. 'Liquid Handling' for the deposition of the sample to test on the 3D-MicroArray filter material and next transporting it alternately up-down through this material.
2. 'Sample Conditioning' for all the physical interactions towards the sample to guarantee

undisturbed reaction progress and signal observation.

3. 'Measurement & Data Handling' for measuring of the fluorescence intensity over the 3D-MicroArray and continuously storing it during the course of the reaction.
4. 'Data Reduction and Evaluation' for the software algorithms that filter the relevant cell intensity figures from the 3D-MicroArray fluorescence pictures.

It is the purpose of this work to come to an adequate solution for the "Sample Conditioning" function by defining, specifying, designing and also theoretically and experimentally confirming an incubator that will account for this function. This incubator must take full advantage of the features of the 3D-MicroArray and must therefore comply with the physical conditions necessary to bring them out.

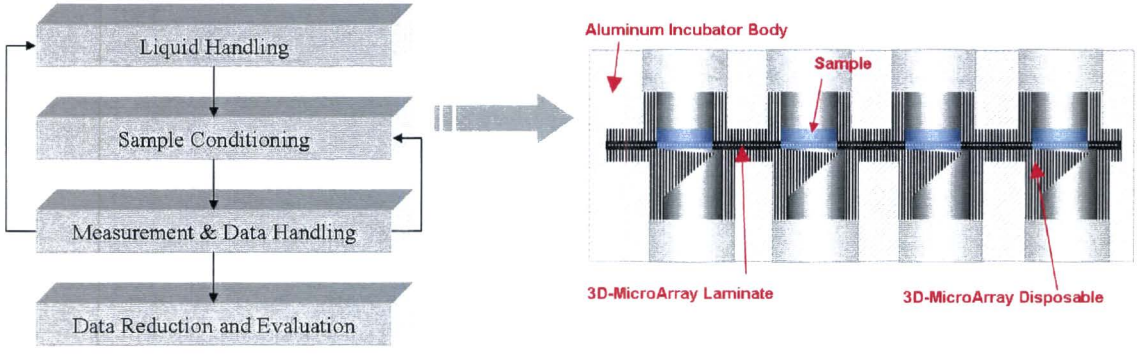

Figure 7
3D-MicroArray System Layout (left) and minimal setup of Sample Conditioning Module (right).

This means, as we see from Figure 7 (left), that interactions with the other function blocks as for instance the "Measurement & Data Handling" module have to be considered. Also from Figure 7 (right) it is clear that the incubator has to physically accommodate the 3D-MicroArray laminate (see Figure 3), as it is sandwiched between a disposable polycarbonate cover and support, both necessary to prevent the samples from contaminating the (most probably aluminum) incubator body.

II CONCEPTUAL DESIGN OF A 3D-MICROARRAY INCUBATOR

1 Specifications

In line with the considerations given in the previous chapter the basic requirements for the 3D-MicroArray Incubator can be derived as follows:

1. The incubator should allow for real time recording, through a fluorescence microscope, of consecutive pictures from and during the hybridization processes on the 3D-MicroArray.
2. During an observation the incubator has to accommodate the 3D-MicroArray with a temperature trajectory at choice somewhere between 25↔75 °C.
3. In no way the sample under investigation must inadvertently be influenced such that the observations become unreliable.

The first requirement boils down to 2 geometrical aspects both concerning a relation between object-lens and membrane, namely: restrictions with respect to their mutual distance and the necessity of a free outlook from the one onto the other.

The second requirement manifests itself in the necessity to make the heat controller programmable. Likewise important is the dynamic behavior of the system. The maximum temperature slew rate of the incubator, positive as well as negative, must not limit the response speed capabilities of the 3D-MicroArray.

Although the third requirement is very generally put, there is one aspect that stands out. Given the rather high maximum temperature demanded for the incubator in combination with the wanted visibility a high evaporation rate can be expected. With *Stefan's law* it can be estimated that at 25 °C the total sample (25 µl) will evaporate in ca 30 seconds given a cylindrical 2 cm long aperture above and of the same diameter as the micro array. At 75 °C the sample will evaporate in a mere 2 seconds.

A glass cover in combination with a narrow channel for pressure equalization is the obvious countermeasure to avoid excessive evaporation. Drawback of this solution is the cold spot that under certain conditions will develop in this glass cover right over the 3D-MicroArray. This may lead to condensation of water vapor there, thus preventing a free sight from the microscope upon it. For that reason (accepting that a glass cover is unavoidable) it is an indirect requirement that the temperature distribution in the incubator will be such that this cold spot temperature will always equal or surpass sample temperature.

2 Basic Concept of a 3D-MicroArray Incubator

Analyzing the combination of requirements as presented in the previous paragraph it only can be concluded that in addition to the set-temperature for the sample under investigation also the temperature gradient inside the incubator has to be controlled. Figure 8 shows the basic concept of such an

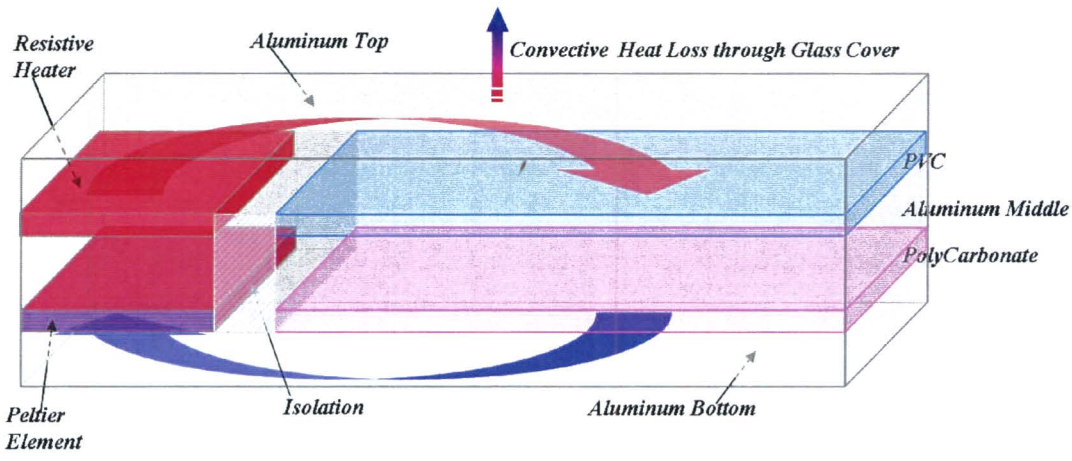

Figure 8
Schematics of a Gradient Incubator

incubator. In a closed aluminum heat flow circuit, on one side next to a resistive heat source, a heat pump (Peltier Element: PE) can be found. On the other side the micro array device (basically a 2 mm thick sheet of polycarbonate) is located together with a sheet of PVC that serves as a heat resistor. All outside surfaces except the top one are supposed to be fully insulated. In stationary use the Resistive Heater (RH) compensates for the convective heat loss through the top as the PE pumps around just as much heat as is necessary to create the wanted temperature difference between top and sample area of the incubator.

At first sight this incubator has a significant drawback. As a PE is not a 100% ideal heat pump it has a collateral heat production. Therefore its circulating heat flow to obtain the adequate temperature difference, should be chosen as low as possible. On the other hand accepting a high heat resistance for the PVC sheet will lead to a high response time for the system given the heat capacitance of the aluminum blocks. In paragraph III3 and chapter IV we will address the possibility to reverse the heat flow through the PE and investigate to what extent, especially in the heating up phase, this will prevent a slow down of the heat dynamics of the 3D-MicroArray Incubator.

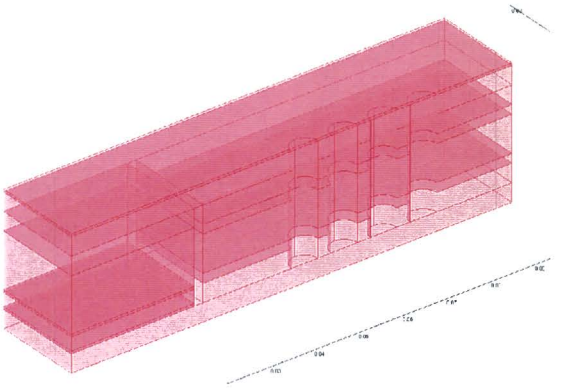

a) Incubator Layout, 38.5x100x20

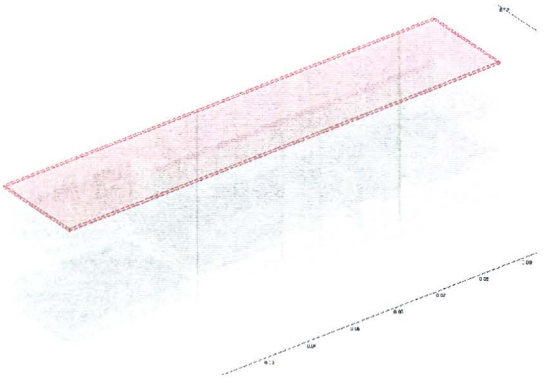

b) Glass Cover, 0.5x100x20

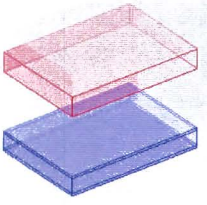

c) RH & PE
RH:4x28x20, $PE_{element}$: 3x28x20, $PE_{Top\&Bottom}$:0.5x28x20

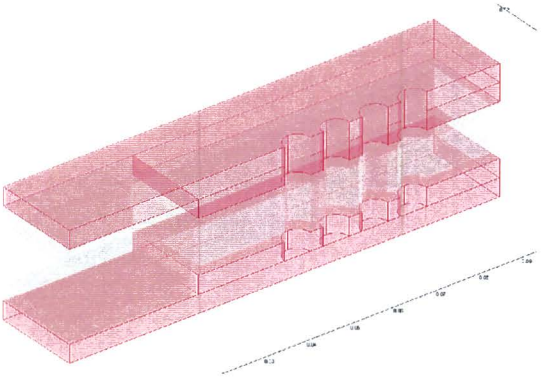

d) Aluminum Top & Bottom: 4x100x20/4x70x20

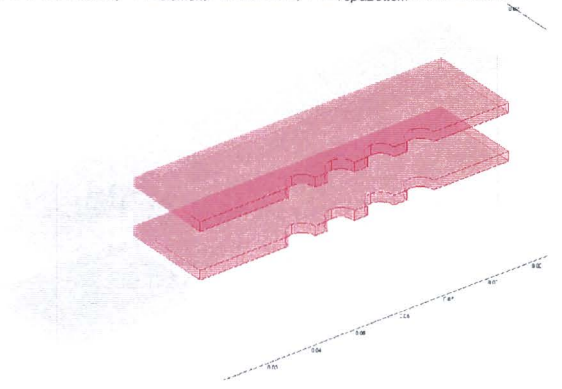

e) PVC Sheet & Polycarbonate Micro Array 2x70x20

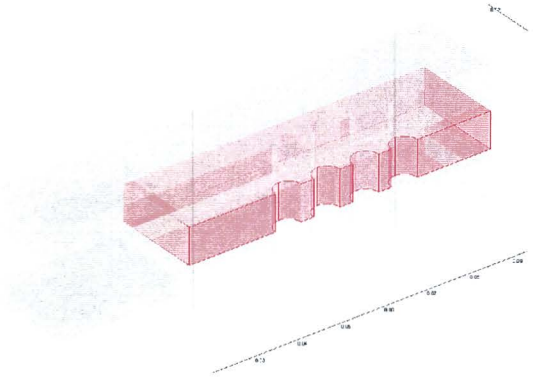

f) Aluminum Temperature Equalizer 8x70x20

Figure 9
(Half) 3D-MicroArray Incubator & Components.
Fronting plane of symmetry. Dimensions HxWxD in mm

III MODELING THE 3D-MICROARRAY INCUBATOR

1 Introduction

Based on the requirements, which follow from the foreseen methods of use of the 3D-MicroArray, a conceptual design for the incubator has been presented in the previous chapter. A major aspect of this design is the approach to control the temperature as well as the temperature gradient to avoid possible condensation in a cold spot on the glass cover surface above the 3D-MicroArray. In this chapter a more detailed 3D-model of this gradient incubator will be presented and used for numerical calculations.

2 Settings for the 3D-MicroArray Incubator Model

Figure 9 shows the composition and dimensions of (half) the incubator. In that figure picture a) gives an impression of the assembled device while pictures b) to f) present the compiling parts. For the model calculations it is supposed that al parts fit together perfectly and that no air gap hinders heat transport. As mentioned before: With exception of the top, where free convection is supposed, all the surface areas of the incubator are 100% insulated. For the various parts the relevant physical characteristics

Character-istics / *Incubator Part*	*Material*	*Thermal Conductivity* κ (W / m K)	*Density* ρ (kg / m^3)	*Specific Heat* C_p (J / kg K)
Top, Bottom, Equalizer RH	*Aluminum*	*160*	*2700*	*900*
Peltier [1] ***Top&Bottom***	*Al-Ceramic 96%*	*35.3*	*3570*	*837*
Element	*Bismuth-Telluride*	*1.5*	*7530*	*544*
Micro Array Device	*Polycarbonate*	*2.0*	*1200*	*1200*
PVC Heat Resistor	*Polyvinylchloride*	*0.16*	*1390*	*980*
Cover	*Glass*	*0.8*	*2580*	*795*

Table 1 Micro-ArrayIncubator Material Characteristics[3]

are chosen as depicted in Table 1. The functioning of the active elements, the RH and the PE, is modeled through adequate settings for the heat source density in the respective domains as follows.

1. For the RH this means that in the incubator model the applied power P_{RH} finds expression in a heat source density $q_{RH} = P_{RH} / V_{RH}$ where V_{RH} stands for the volume of the RH domain (see

[1] **Melcor** 1040 Spruce Street – Trenton, NJ 08648 USA

Figure 9c) and equals .004x.028x.04=4.48 10^{-6} m^3 for the total incubator, so $q_{RH} = P_{RH} / 4.48\ 10^{-6}$ W / m^3.

2. Modeling the PE is slightly more complicated. From Figure 10 we can learn that in the

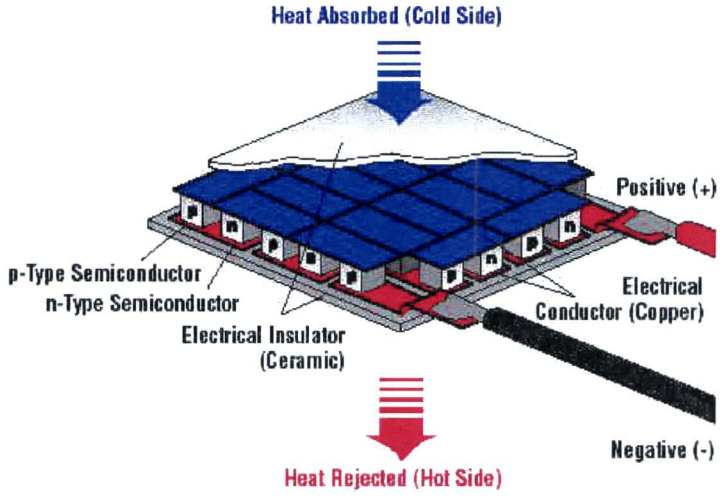

Figure 10 Peltier Element, exploded view.

PE three domains can be distinguished: In the middle we see the material that exhibits the actual Peltier effect and consists of a number of small pillars of alternately p-type and n-type semi conducting material (e.g. Bismuth-Telluride), electrically connected in series, but thermally arranged in parallel. On top and bottom there are two identical sheets of Al-ceramic material that inhibits electrical current, but conducts heat very well. It is assumed that no significant heat transport takes place through the air slits between the pillars. For the PE[2] used in the incubator this domain is then characterized as follows (see for detailed dimensions also Figure 11 and Figure 9):

As there are N=127 pillar pairs of p- and n-type Bismuth-Telluride (κ =1.5 W / m K) and as those pillars have a (cross-section / height)-quotient: G=6.1 10^{-4} m and a height: L=3.6 mm, then the PE device has a thermal conductance $K_{PE} = 2N\kappa\ G = 0.23$ W / K . This means that for the PE_{Body} domain, as depicted in Figure 11, the equivalent specific heat conductance $\kappa_{PE} = K_{PE}$ x 0.003 / (0.028 x 0.040) = 0.616 W / m K.

[2] **Melcor** CP 1.0-127-06

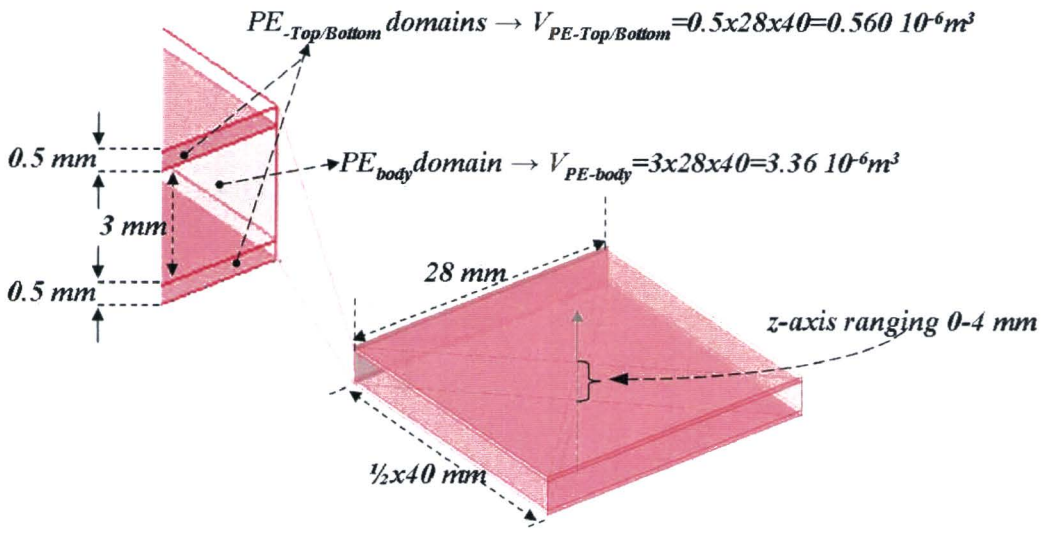

Figure 11
Peltier Element: Model Layout.

The ohmic resistance of the PE equals $R_{PE} = 4.6\ \Omega$. The electrical current I_{PE} through the PE_{Device} is not only accountable for the heat pump effect but also generates resistive heat $PR_{PE} = I_{PE}^2.R_{PE}$ W. This effect is incorporated in the model by setting in the PE_{Body}domain an equivalent heat source density of $q_{eq} = I_{PE}^2.R_{PE} / V_{PE\text{-}body}$ or $q_{eq} = 1.37\ I_{PE}^2$ MW / m^3.

In the $PE_{Top\&Bottom}$ domains the Peltier effect finds expression. For this heat source/sink $\pm P_{PE}$ we can write: $P_{PE} = 2$ N a I_{PE} T = 15.4 I_{PE} W (for T= 300K). The factor a is the Seebeck coefficient and equals 2.02 10^{-4} Volt / K for Bismuth-Telluride (for T=300K). Again by setting the heat source density in the concerning domains, these effects can be incorporated in the model as follows: $q_{eq} = 15.4\ I_{PE} / V_{PE\text{-}Top/Bottom} = 27.5\ I_{PE}$ MW / m^3, where this number will be positive at the source and negative on the sink side.

Figure 12 shows the simulation of a PE where it is totally isolated except for the bottom surface at z=0, that is being kept at 25 °C. Both figures show in 5 second steps the development to a stationary situation after the current through the PE has been switched from 0↔2A. At left Figure 12a shows the temperature on the z-axis (see Figure 11) versus the z-position. At right Figure 12b shows the heat flux in the z-direction at the same locations.

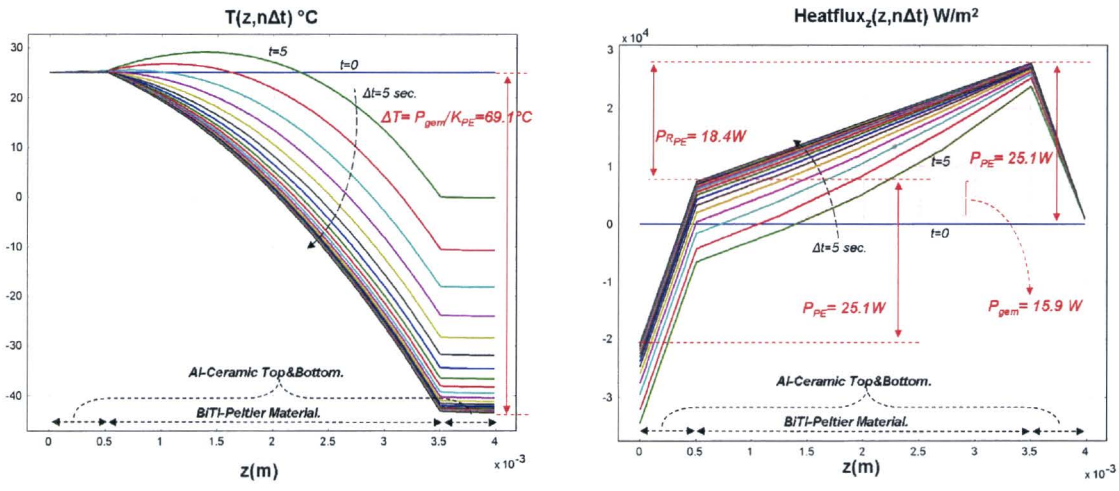

a) *b)*

Figure 12
Temperature (a) and heat flow (b) in Peltier Element[2] , I_{PE}=2A, t=0↔100s[3]

The physical interpretation of the curves of Figure 12 proofs the validity of the simulation results. The curves in the stationary situation show how the Peltier heatflow comes up in the Al-ceramic top and bottom material of the device and how the Peltier-resistive power manifests itself in the linear slope of the flux curve in the BiTI region. Taking the mean heatflow over the Peltier material and deviding it by the heat conductance gives the temperature over the Peltier element and is fully in accordance with the simulation results.

3 Modeling Results for the 3D-MicroArray Incubator

With **Femlab 3.0** (Copyright © by COMSOL AB) the thermal behavior of the 3D-MicroArray Incubator as depicted in the previous paragraph has been simulated (appendix III). Time dependencies of the settings for the RH and the PE where chosen such that a good impression could be obtained of the heating-up dynamics of the 3D-MicroArray. The model layout has already been depicted in Figure 9 with data for the material characteristics as in Table 1 and the concerning paragraph.

To test the underlying reasoning the 3D-MicroArray Incubator has first been simulated without putting the PE module into practice. With no circulating heat flow and with the PVC heat resistance replaced by a similar aluminum part we get results as depicted in Figure 13. The figure b) at the right shows the temperature trajectories for three points in every cuvet on locations as marked in the bottom left picture c). The four locations in the middle of the cold spots on the glass surface show a ca 3 °C lower

[3] Simulated with **Femlab 3.0** Copyright © by COMSOL AB.

temperature when compared with the adjacent aluminum cuvet walls, this in a situation with a mode-

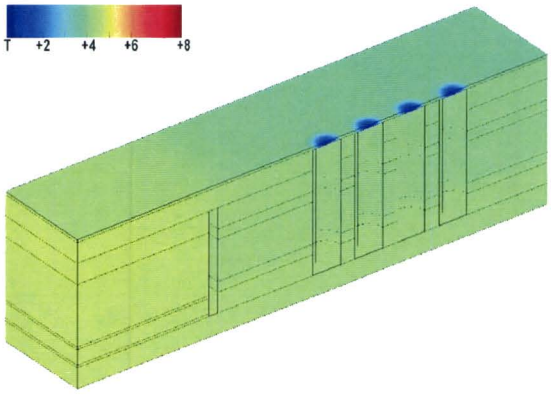

a) Temperature distribution at t=990s

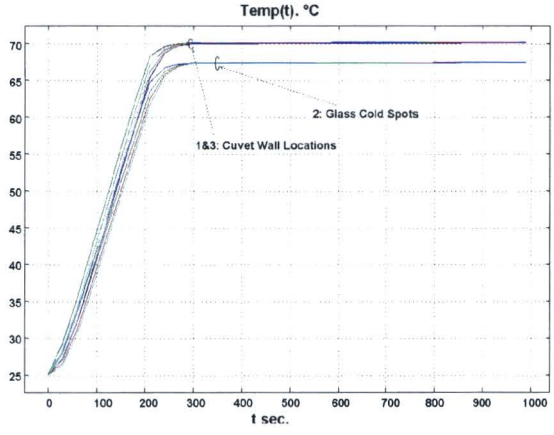

b) Temperature curves in cuvettes.
For locations 1,2 and 3 see c).
(At t=200s RH switches from 60 to 1.86 W)

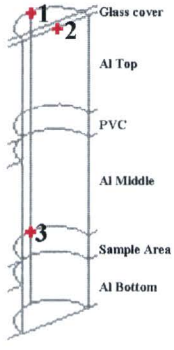

c) Measurement positions per cuvette.

Figure 13
3D-MicroArray Incubator without PVC heat resistor. Heating up scenario without PE.

rate convective cooling of h=10 W/(m^2 K) via the top glass cover.

The temperature dent in the glass cover over the cuvet can be approximated as follows:

$$\frac{dT}{dr} \approx \frac{\pi r^2 \cdot h \cdot \Delta T_{Top \to Ambient}}{2\pi r \cdot \kappa_{glass} \cdot d_{glass}} \qquad (1)$$

For a cuvet diameter of 6mm, κ_{glass} = 0.8W/mK, ΔT = 50°C and d_{glass} = 0.5mm this leads to a temperature dent of 2.8 °C which is in good accordance with the model results.

The color in the top left picture a) represents the incubator temperature at the end of the trajectory (t=990s), spanning (from blue to red) a range of 8°C. Except for in those cold spots a rather good homogeneity can be observed.

After restoring the PVC heat resistance, warming up the incubator takes considerably longer and we get the situation as shown in Figure 14 (again without a circulating heat flow as normally will be the case) where the equilibrium temperature distribution is much the same as in the previous situation.

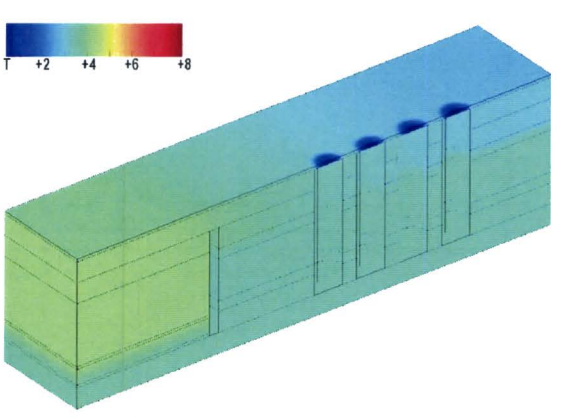

a) Temperature distribution at t=990s.

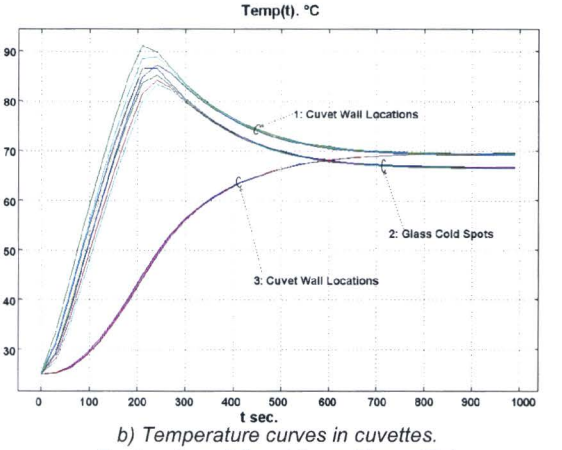

b) Temperature curves in cuvettes.
For locations 1,2 and 3 see Figure 13c)
(At t=200s RH switches from 60 to 1.86 W)

Figure 14
3D-MicroArray Incubator with PVC heat resistor.
Heating up scenario without PE.

As already suggested in the previous chapter the PE module will almost eliminate this time delay effect when its use is being extended to an active regulating one. Instead of being limited to generating a constant, circulating, background heat flow, the PE module has to be controlled such that a constant temperature difference will arise between the glass cover cold spot and the corresponding sample. From Figure 14b we can learn that in that case up to somewhere t=400s the PE module actively would transport heat generated by the RH downwards to the sample area from beneath, in fact avoiding the PVC heat resistance. Figure 15 shows the results of a simulation with a scenario for RH and PE settings that mimic such active control. The results confirm the expectations. The heating up of the 3D-MicroArray Incubator exhibits an almost identical pattern as compared with the situation with the PVC heat resistance removed as shown in Figure 13. Quite different results come out this comparison in the stationary phase: As expected the temperature in the sample area is now, thanks to the PE generated circulating heat flow, clearly under the temperature in the glass cover cold spot.

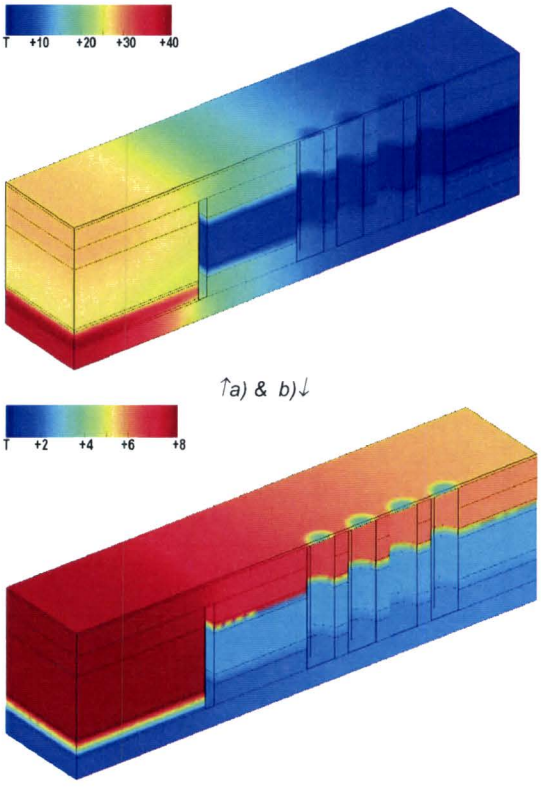

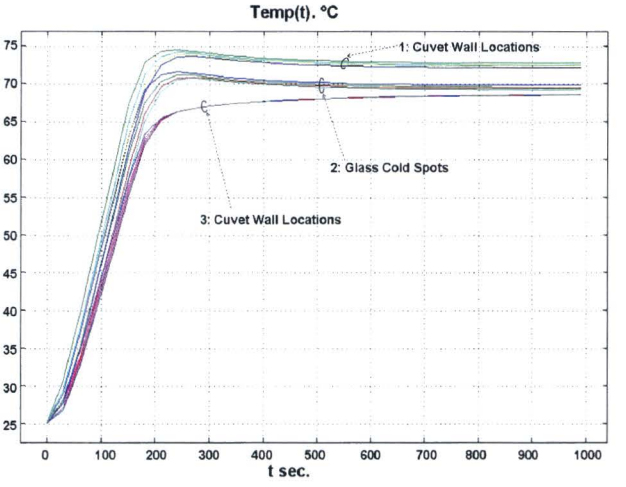

c) Temperature curves in cuvettes.
For locations 1,2 and 3 see Figure 13c)
(At t=158s RH switches from 60 to 1.86 Watt and
PE switches from 28.5 to -2.4 Watt)

←Temp. distribution at a) t=120s and b) t=990s

Figure 15
3D-MicroArray Incubator with PVC heat resistor.
Heating up scenario including PE.

From the above we can conclude that the outcome of the model studies in this chapter confirms the feasibility of the design of the 3D-MicroArray as specified and developed in chapter II.

IV CONTROLLING THE 3D-MICROARRAY INCUBATOR

1 Introduction

In the previous chapters the specifications for and the concept and design of the 3D-MicroArray Incubator have been elucidated and evaluated. Based on 3D model calculations we were able to conclude that the presented design indeed can satisfy the prerequisites as formulated. To obtain a coherent approach as how to address the specific elements when controlling the overall functioning of the 3D-MicroArray Incubator, the Simulink® platform for multidomain and model-based design of dynamic systems has been used. Simulink® provides an interactive graphical environment and a customizable set of block libraries that enable accurate design, simulation and implementation of time-varying systems. Because Simulink® is integrated with MATLAB® real time applications can be realized using PC input/output facilities. The BLN group at the Physics department at the TU/e used these possibilities to develop hardware (TUeDACS/1 QAD) and software (Wintarget®) to let Simulink® models run in real-time. Such a Simulink® model used in combination with this TU/e hard- and software has very much facilitated the experimental evaluation of the 3D-MicroArray Incubator.

2 A Dynamic System Model of the 3D-MicroArray Incubator

In the previous chapters, details in the temperature distribution in the 3D-MicroArray Incubator were especially looked at. Small details, notably in the foreseen glass cover, were considered to be eventually of major importance. 3D numerical model computations showed to what extent those small details indeed could influence the working of the 3D-MicroArray Incubator, but also how bringing about a simple temperature gradient could avoid unacceptable consequences. At the same time it was shown that the response time deterioration emanating from this solution most likely could be avoided by an extended control of the PE.

To further look into this approach we go back to the schematics of a gradient incubator as depicted in Figure 8. For this gradient incubator a simplified equivalent dynamic layout encompassing the relevant components is presented in Figure 16. This circuit includes a straightforward modeling of the PE with a heat pump shunted by a heat conductance. The resistive heat development in the PE is represented by 2 equally powered heat sources each connected to its own end of the PE's heat conductance.

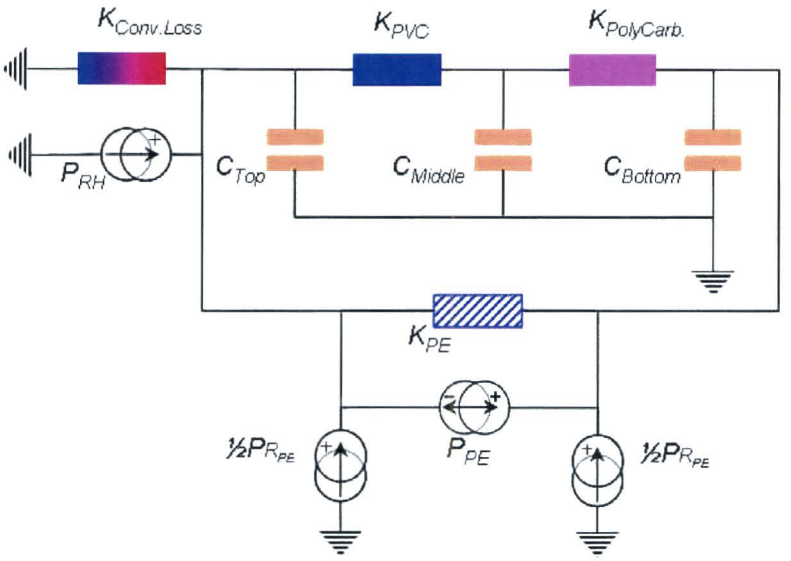

Figure 16
Replacement circuit for the 3D-MicroArray Incubator.

In Table 2 the numerical values of the components of the heat circuit for the 3D-MicroArray Incubator are shown. Computations are based on the material characteristics as given in Table 1 and the geometrical layout of the incubator as depicted in Figure 9.

$K_{Conv.Loss}$	$ht(W/Km^2)*Width_{TopSurface}(m)*Depth_{TopSurface}(m)$ $10*0.1*0.04$	0.04	W/K
K_{PVC}	$k_{PVC}(W/Km)*(Width_{Middle}(m)*Depth_{Middle}(m)-4*pR^2_{Cuv})/Height_{Middle}(m)$ $0.16*(0.07*0.04-4p0.003^2)/0.002$	0.215	W/K
$K_{PolyCarb.}$	$k_{PolyCarb}(W/Km)*(Width_{Bottom}(m)*Depth_{Bottom}(m)-4*pR^2_{Cuv.})/Height_{Bottom}(m)$ $2.0*(0.07*0.04-4p0.003^2)/0.002$	2.69	W/K
K_{PE}	See chapter III paragraph 2.	0.23	W/K
C_{PE}	$V_{PE}(m3)*\rho_{BiTe}(kg/m3)*Cp_{BiTe}(J/kgK)$ $3.36\cdot10^{-6}*7530*544$	13.8	J/K
C_{PVC}	$V_{PVC}(m^3)*\rho_{PVC}(kg/m^3)*Cp_{PVC}(J/kgK)$ $5.6\cdot10^{-6}*1390*980$	7.6	J/K
C_{PolyC}	$V_{PolyC.}(m^3)*\rho_{PolyC}(kg/m^3)*Cp_{PolyC}(J/kgK)$ $5.6\cdot10^{-6}*1200*1200$	8.06	J/K

C_{Top}	$V_{Top}(m^3)* \rho_{Al}(kg/m^3)*Cp_{Al}(J/kgK)$ $44.22 \cdot 10^{-6}*2700*900+½\ C_{PVC}+½\ C_{PE}$	118.15	J/K
C_{Middle}	$V_{Middle}(m^3)* \rho_{Al}(kg/m^3)*Cp_{Al}(J/kgK)$ $26.75 \cdot 10^{-6}*2700*900+½\ C_{PVC}+\ C_{PolyC}$	60.08	J/K
C_{Bottom}	$V_{Bottom}(m^3)* \rho_{Al}(kg/m^3)*Cp_{Al}(J/kgK)$ $21.5 \cdot 10^{-6}*2700*900+\ C_{PolyC}+½\ C_{PE}$	75.93	J/K
P_{RH}	Adjustable	$0 \leftrightarrow 60$	W
P_{PE}	Adjustable	$-40 \leftrightarrow +40$	W
PR_{PE}	$R_{PE}(O)*\{P_{PE}(W)/[2*N*a(V/K)*T(K)]\}^2$ $4.6*\{P_{PE}/[2*127*2.02 \cdot 10^{-4}*300]\}^2$	$1.94 \cdot 10^{-2}(P_{PE})^2$	W

Table 2
Values for the components used in the replacement circuit for the 3D-MicroArray Incubator

The dynamic circuit layout of the 3D-MicroArray Incubator from Figure 16 is used as starting point for the Simulink® model as represented in Figure 17 and in more detail in appendix IV.

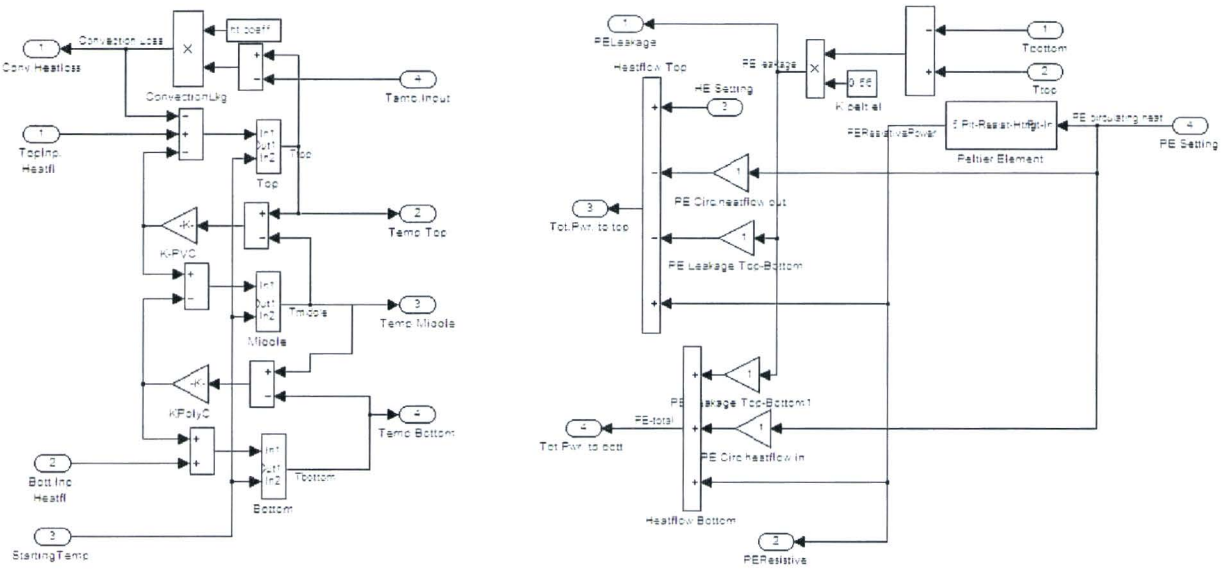

a) Aluminum Heat Flow Circuit. *b) Resistive Heater and Peltier Element.*

Figure 17
Simulink® Dynamic System Model of 3D-MicroArray Incubator

To study the validity of this simplified approach equivalent scenarios were calculated as with the 3D-Femlab® model as described before in chapter III. The results are shown in Figure 18 and suggest a

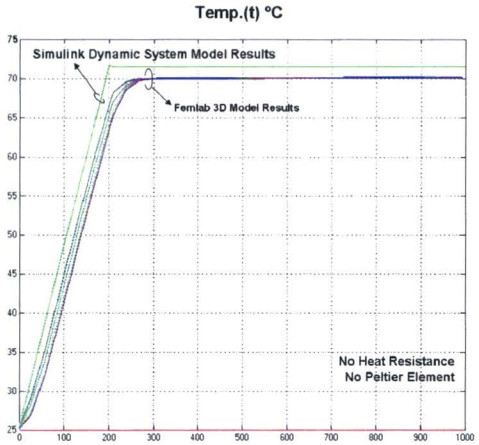

a)

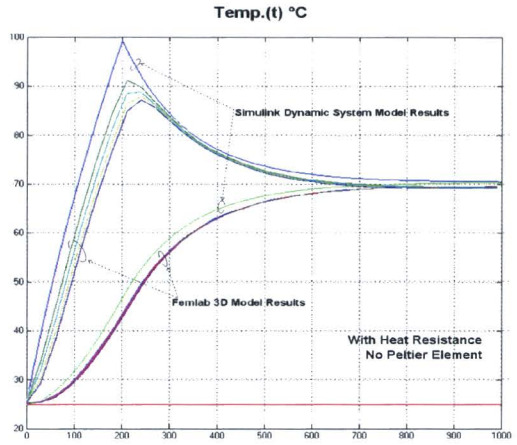

b)

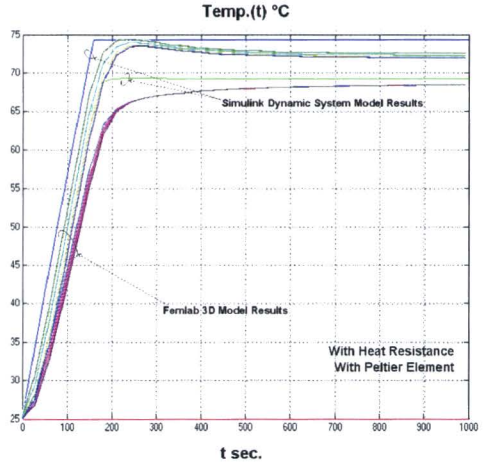

c)

Figure 18
Comparison of results of Femlab® 3D model and Simulink® Dynamic-System model. Both models and all scenarios: $T_{ini}=T_{amb}=25°C$

a) At t=200s RH switches from 60 to 1.86W.
b) At t=200s RH switches from 60 to 1.86W.
c)At t=158s RH switches from 60 to 1.86W and PE switches from 28.5 to -2.4W

more than acceptable conformity as well in magnitude as in timely behavior.

3 Control of the 3D-MicroArray Incubator

To better understand the timely behavior of the 3D-MicroArray Incubator the circuit of Figure 16 can be simplified even further as represented in Figure 19 a) and b). In a) the components of the original replacement circuit are rearranged and power sources are combined for as far as possible. Five time-constants come out as depicted in Table 3. As τ_2 and τ_4 are each more than 10 times less than

$\tau_1 = C_{middle} / K_{PVC} = 279$ s
$\tau_2 = C_{bottom} / K_{PolyCarb.} = 28.2$ s
$\tau_3 = C_{top} / K_{PVC} = 539$ s
$\tau_4 = C_{middle} / K_{PolyCarb.} = 22.3$ s
$\tau_5 = C_{bottom} / K_{PE} = 330$ s

Table 3
Time-constants in 3D-MicroArray Incubator

τ_1, τ_3 and τ_5 it can be concluded that $K_{PolyCarb.}$ is of a negligible magnitude. Therefore $K_{PolyCarb}$ can be spread over K_{PVC} and K_{PE}. As a consequence C_{bottom} and C_{middle} can be combined to $C_{Comb.}$ and also $1/(1/K_{PVC}+1/[2.K_{PolyCarb}])$ and $1/(1/K_{PE}+1/[2.K_{PolyCarb}])$. This leads to the circuit of Figure 19b) with

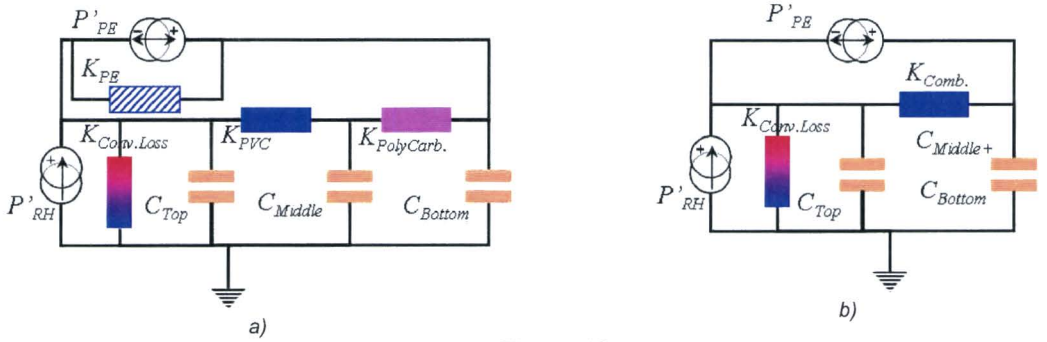

Figure 19
Simplified Circuits for 3D-MicroArray Incubator

$K_{Comb.}$=0.430 W/K and $C_{Comb.}$=136J/K.

The time-constant $\tau_{Comb.}=C_{Comb.}/K_{Comb.}$=316s and is clearly recognizable in Figure 18b. Figure 18c shows the effect of the PE. Provided the steering of the PE keeps step with both the temperatures in the top and middle compartment of the incubator, the effect of $\tau_{Comb.}$ can be effectively suppressed. Figure 19b helps to understand this phenomenon: in fact with a correctly controlled PE the heat resistance $1/K_{Comb.}$ is virtually short-circuited.

From the reasoning above it is clear that the controller of the 3D-MicroArray Incubator has to include the PE. Instead for delivering a constant background of circulating heat, the PE has to be used to distribute heat generated by the RH to the top, middle and bottom compartment in such a way that the temperatures of those compartments closely follow each other in accordance with the desired temperature gradient settings.

Concerning the above, the obvious approach is to control the RH on the basis of the difference between the desired and the actual temperature of the sample area in the middle compartment of the incubator. At the same time the PE is controlled such that the temperature gradient between the top- and the middle-compartment of the incubator follows a trajectory given by $(T_{Top}-T_{Middle})/(T_{Top}-T_{Amb.})$=const. T_{Top}

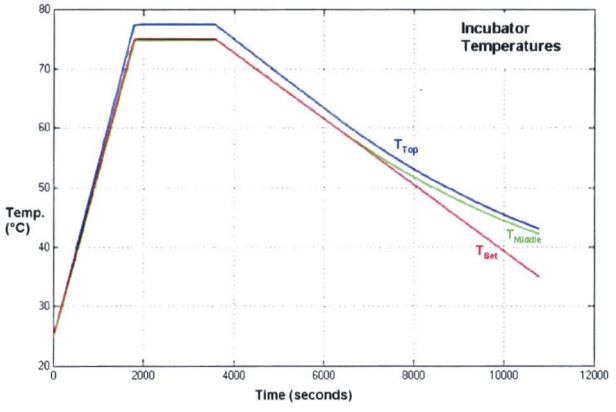

a) T_{top}, T_{middle} vs T_{set}

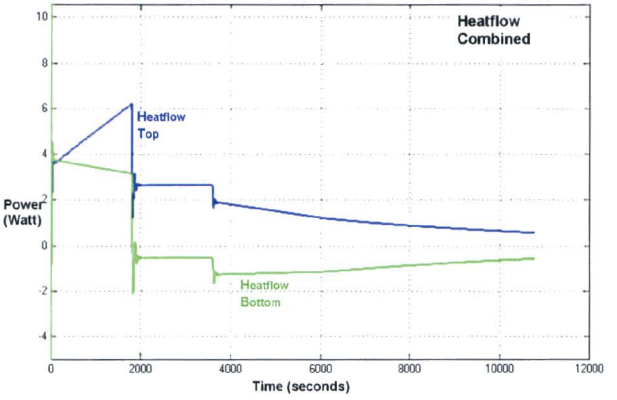

b) Heat flow towards Incubator-Top and -Bottom

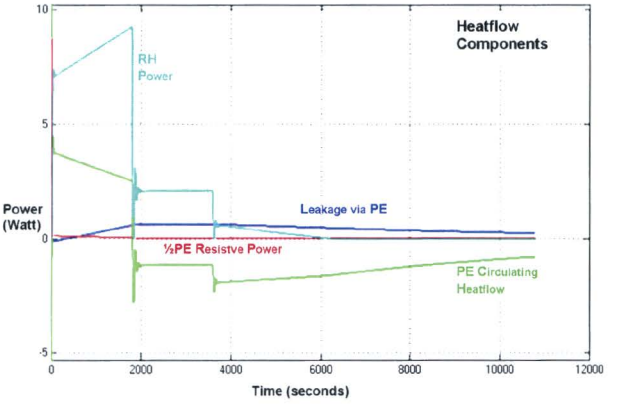

c) Components of Incubator Heat flow.

Figure 20
Controlling the 3D-MicroArray Incubator

and T_{Middle} are continuously being measured. $T_{Amb.}$ is an input variable and is set to the ambient temperature where as *const.* determines the magnitude of the temperature gradient and has to be set in relation to the expected cold spot temperature. Standard settings are $T_{Amb.}$=25°C and *const*=0.05 for a temperature gradient of ~3°C between the top and middle compartment at T_{Top} =75°C.

In Figure 20 the working of the 3D-MicroArray Incubator is represented in detail in the graphs resulting from a Simulink® simulation with the above described incubator model and control.

In b) and c) it is clearly shown that in the warming up phase the PE control effectively short circuits the PVC heat resistance and that a part of the by the RH generated heat is being led into the opposite direction via the bottom area to the sample region, in the middle of the incubator.

Moreover in a) we see how the trajectory of the desired temperature T_{Set} is being followed by both the top and the middle region of the incubator. In the down slope part of this T_{Set} trajectory we see however that from around t = 7000 (sec.) cooling is insufficient and deviations start to occur. From this moment on the RH is being shut down by its controller as can be concluded from figure c) whereas the control for the PE is still active and maintains the desired temperature gradient.

V EXPERIMENTS

1 Technical Construction

The functional setup and layout of the 3D-MicroArray is represented in Figure 9 and serves as basis for the technical realization as shown in Figure 21.

At the right we have the passive part of the incubator packet. This packet consists of:

1. Glass cover preventing sample evaporation
2. The aluminum top to connect to the top of the heater packet
3. The PVC sheet acting as heat resistor
4. The aluminum middle to flatten temperature differences in the region of the micro arrays
5. The polycarbonate sheet representing the disposable 3D-MicroArray and
6. The aluminum bottom to connect to the bottom of the heater packet.

This part of the incubator is assembled with 4 metal through going bolts. Spring cups are provided to control the resulting tension between these parts of the construction.

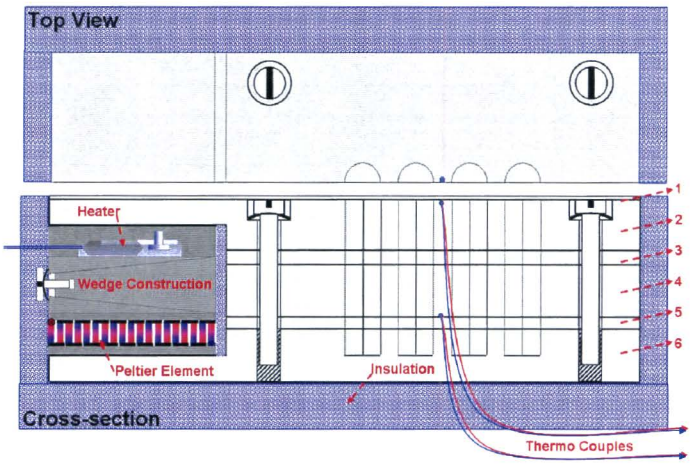

Figure 21
Cross-section and top view of 3D-MicroArray Incubator construction

At the left we have the active heater packet that comprises:

1. An N-Channel Power MOSFET mounted on an aluminum block functioning as a controllable Resistive Heater
2. An aluminum wedge construction with a (spring loaded) bolt making the heater packet height-

adjustable and controlling the counter pressure within the heater packet when mounted and

3. A Peltier Element serving as a heat pump.

With the wedge construction the heater packet is clamped between the prongs of the fork made up by the extending parts of the aluminum top and bottom of the incubator packet, thus closing the heat flow circuit and enabling a circulating heat flow.

For the control of the incubator 2 temperature sensors (Iron/Constantan thermocouples) have been introduced (see Figure 21)

2 Driver Circuitry

Heating

The electronic driver circuits for the RH and the PE are given in Figure 22 left (RH-driver) and right (PE-driver).

In the RH-driver the power MOSFET (IRF540 located in the RH, see Figure 21) carries current from 'earth' to R_L according to: $I_{FET}=-V_{watt}\cdot(R_2/R_1)/R_L$ assuming $R_1=R_3$ and $R_2=R_4$. Given $(I_{FET}\cdot R_L)<<|V^-|$ it follows that $P_{FET}\equiv RH_{power}\approx I_{FET}\cdot|V^-|$ and is directly proportional to V_{watt} for $V_{watt}\geq 0$.

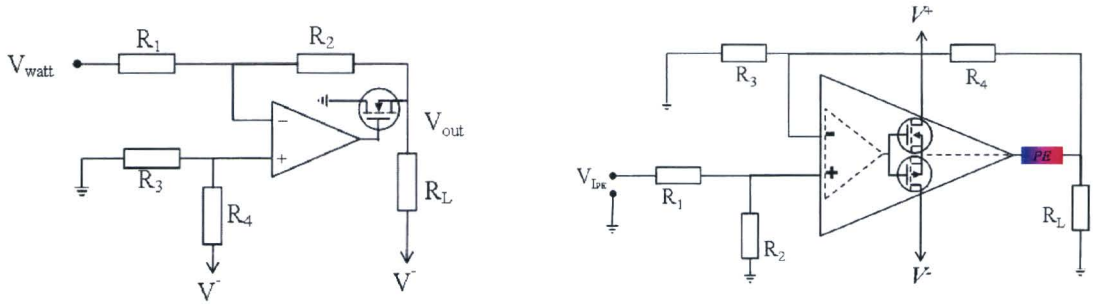

Figure 22
Driver for the Resistive Heater (left) and Peltier Element (right)

In the PE-driver a with a pair of complementary power MOSFET's (IRF540-IRF9540) boosted op-amp controls the current through the PE in an equivalent way according to $I_{PE}=V_{IPE}\cdot(R_2/(R_1)/R_L$.

Sensing

In the 3D-MicroArray Incubator 2 J-type (Iron/Constantan) thermocouples are foreseen (see Figure 21). For reading out an AD594 IC is implemented. This IC is laser trimmed to 1 °C calibration accuracy (at 25 °C) for J-type thermocouples and has a low impedance voltage output of: 10 mV/°C. An ice point compensation is build-in (see Figure 23).

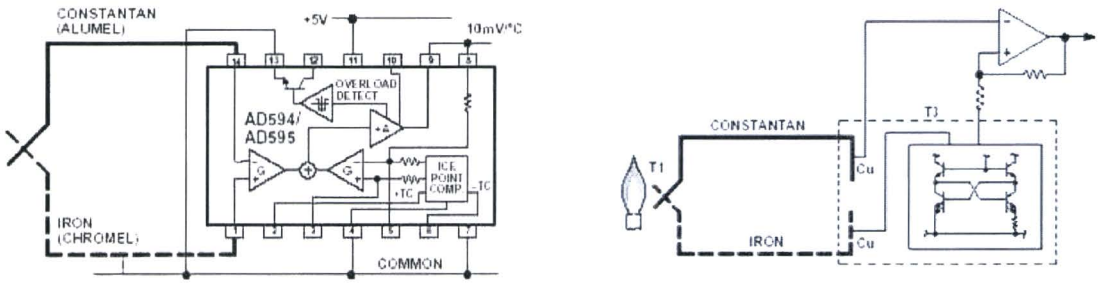

Figure 23
Monolithic Thermocouple Amplifier(AD594, left) with Cold Junction Compensation(right)[4].

3 Coupling to PC

The actual dynamic system model of the 3D-MicroArray Incubator as depicted in Figure 17 is in the final Simulink® program embedded in a set of supporting software blocks that enable the control of its functioning and the logging of its performance as both are being simulated by the program. See Figure 24 (left) and appendix IV.

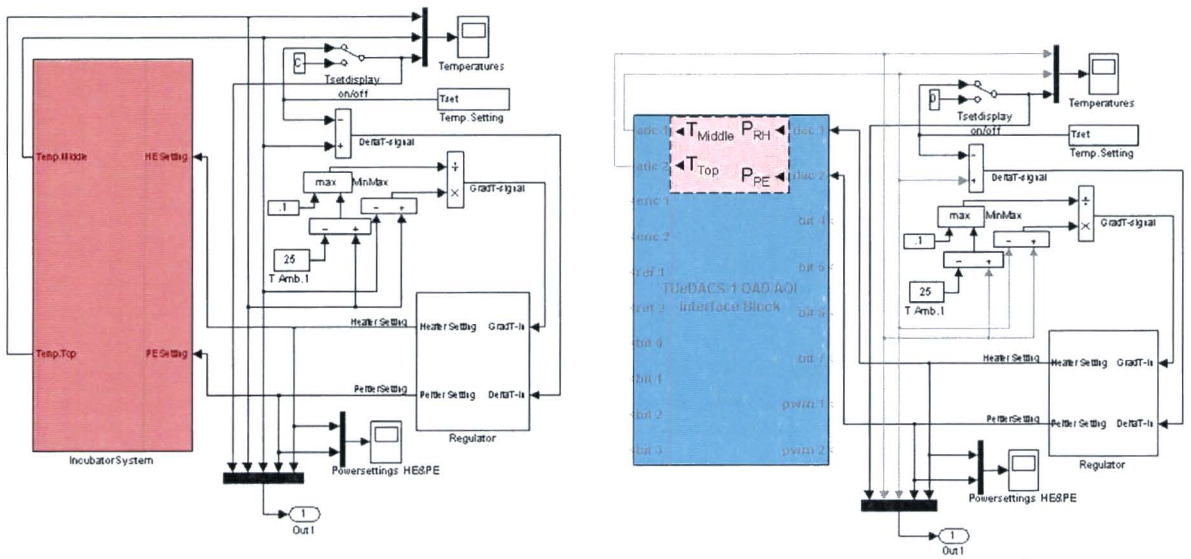

Figure 24
3D-MicroArray Incubator with support functions.
Simulink® model (left), TUeDACS/1 QAD (right).

[4] **ANALOG DEVICES,** Norwood, MA, USA

It is obvious that the physical test setup of the incubator as presented in the previous paragraphs has corresponding input/output functions as compared with its model in Figure 24 (left). As mentioned before Simulink® is integrated with MATLAB® and thus real time applications can be realized using PC input/output facilities. This feature of Simulink® has been used to create a real time function block to substitute the one labeled 'IncubatorSystem' in Figure 24 (left). This function block connects the rest of the Simulink® dynamic system model with the actual 3D-MicroArray Incubator experiment via a TUeDACS/1 QAD as shown in Figure 24(right). Running this model and letting it control the incubator test setup as indicated made it possible to compare theory and practice in a flexible way under circumstances as identical as possible and very much facilitated the experimental evaluation of the 3D-MicroArray Incubator.

4 Measurements

Setup

In conformity with the previous paragraphs an incubator device, driver- and sensor-electronics and cradle of polystyrene foam have been made (see Figure 25). After coupling of this setup via a TUeDACS/1 QAD to a PC, measurements have been carried out to investigate the physical behavior of the incubator.

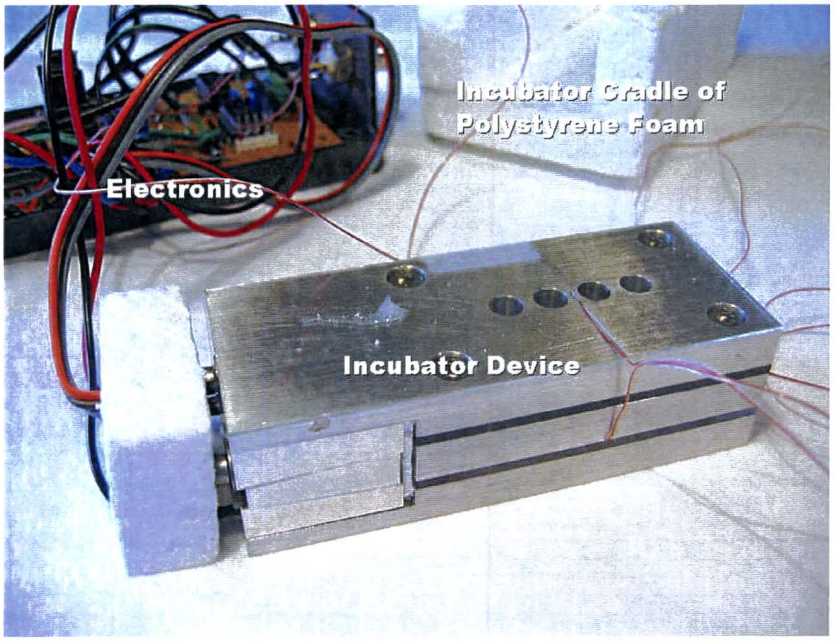

Figure 25
Incubator Set-up.

Calibration

- In Figure 22 the drivers for the RH and the PE accept voltage inputs. These voltage inputs determine the current flow through the RH power-MOSFET and the PE power-MOSFET complementary pair respectively. The conversion factors for both drivers are given in paragraph V2 and comply with the measurement results as depicted in Figure 26. To obtain the actual RH heat production and PE heat flow both factors have to be multiplied by the actual RH power MOSFET drain to source voltage and the concerning 'Peltier Element' factor respectively.

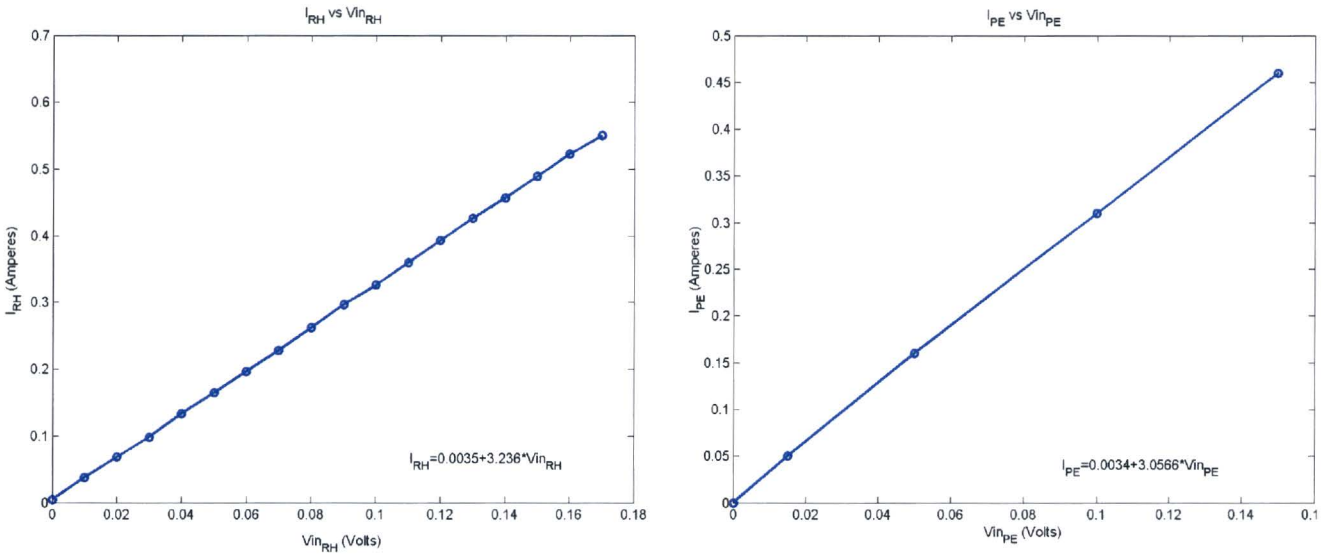

Figure 26. Calibration of driver settings.

- With the incubator in temperature equilibrium at the beginning of a measurement session the eventually temperature offset between both thermocouples was removed with respect to their long term mean as is shown in Figure 27.

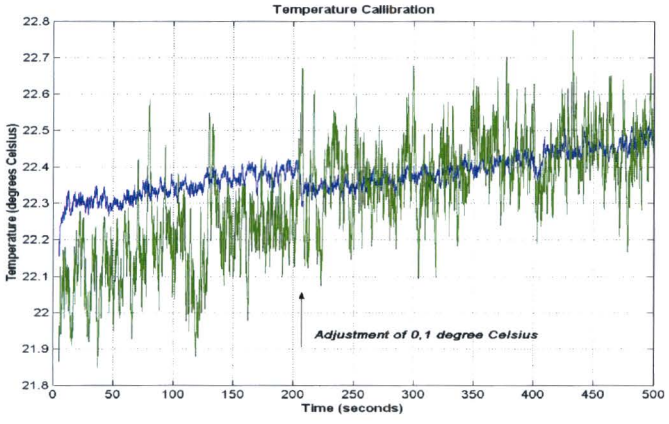

Figure 27
Temperature Offset Setting to match both Thermocouples (Blue=T_{top}, Green=T_{middle})

- From Figure 27 it is clear that both thermocouples have different noise levels. Renewing the connections between both thermocouples and the electronics did not change the situation. Also exchanging thermocouple amplifiers did not make a significant difference. As no further indication could be found suggesting a malfunction of the concerning thermocouple the situation was accepted.

- After heating up to almost 60°C the incubator was left alone and the cooling down was recorded for a period of 500 seconds (see Figure 28). In the range of 50 °C the temperature slope of the top area

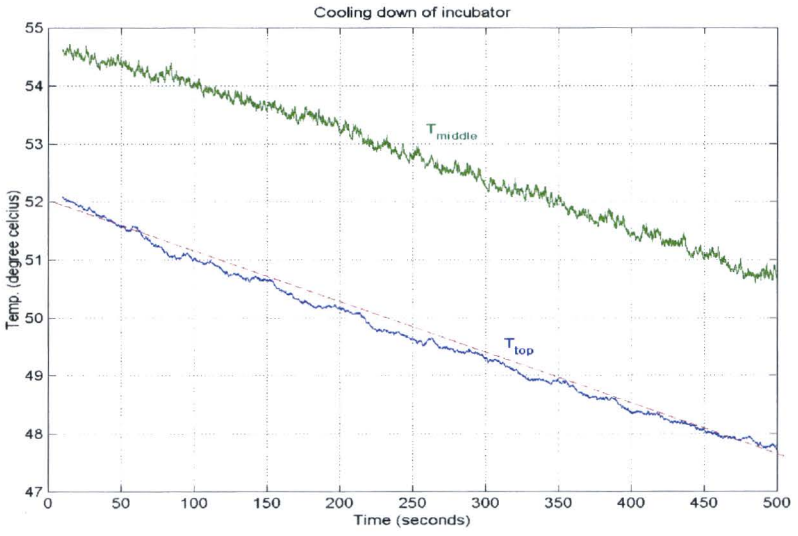

Figure 28
Cooling Down of Incubator

equals 9.10^{-3} °C/s. The heat capacitance of the incubator is known from Table 2 and equals 254 J/K. This means a heat loss of 2.3 W via the top surface area of the incubator. So as the temperature difference to ambient is 25°C and as the concerning surface area measures 0.04x0.1m^2 the actual (combined) heat transfer coefficient can be roughly estimated as:

$$h \approx \frac{2.3W}{25K \cdot 4.10^{-3} m^2} = 23 \frac{W}{m^2 K} \qquad (2)$$

This is in accordance with the estimations given in appendix III2.

Peltier Element

To test the working of the Peltier Element in the incubator setup an alternating moderate heat flow of 4 W at $t \leq 600$ s and -4 W at $t > 600$ s has been applied. Results are presented in Figure 29 and show that

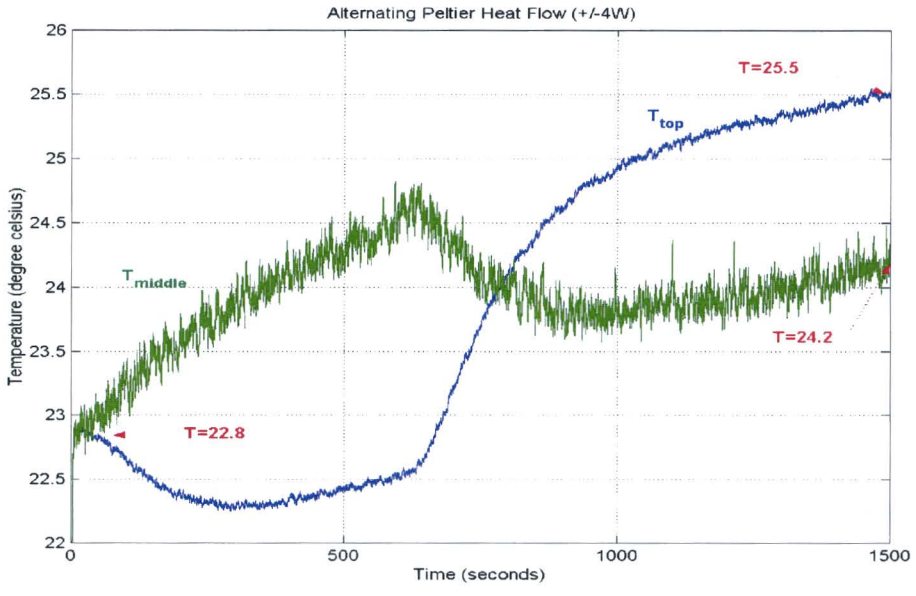

Figure 29
Alternating Heat Flow (switched from +4W to -4W at t=600sec)

the total energy content of the incubator test device has increased at t = 1500 seconds. From Table 2 and Figure 29 it can be derived that this amounts a total of 450 J which corresponds with an energy source of .3 W. This is completely accounted for by the resistive heat production of the Peltier Element that equals $1.94\ 10^{-2} \cdot 4.0^2 = 0.31$ W (see Table 2).

Contrary to this conformity for the resistive heating there is a considerable mismatch between observations and model calculations concerning the circulating heat flow originating from the Peltier Element. In Figure 30 at the left the actual observed temperatures are plotted combined with the corresponding model temperatures. Instead of the actually observed temperature difference of 1.5 °C, the model gives a temperature difference of 8.5 °C after 1500 seconds for the same procedure. An electronics fault is unlikely as the resistive heating by the Peltier Element indeed did meet the expectations. The only plausible explanation seems to be a short circuiting of the PE generated heat flow in or close to the Peltier Element. The diagram in Figure 30 at right represents a situation with the same conditions and procedures except for an 11-fold increase of the internal heat conductance of the Peltier

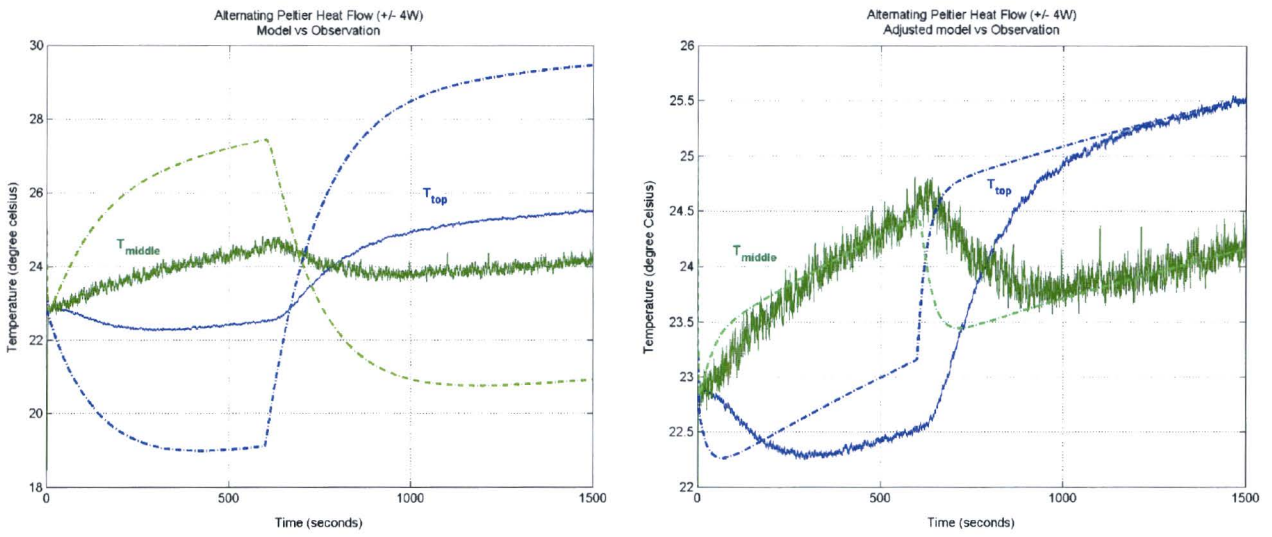

Figure 30
As Figure 29. and in comparison with model computations.
Left with settings for correct working PE, right adjusted in conformity with supposed malfunction. .

Element. The shift of the model results towards the actual observed situation is remarkable. The likelihood and possible physical cause of such an event will be discussed later.

Resistive Heater

The RH in combination with the concept of a temperature gradient incubator was tested with a scenario equivalent to the one of Figure 14 and Figure 18b. Because of driver limitations, heating up power was limited to 15 W with heating up time elongated to 300 seconds. Standby power was set to 0.9 W.

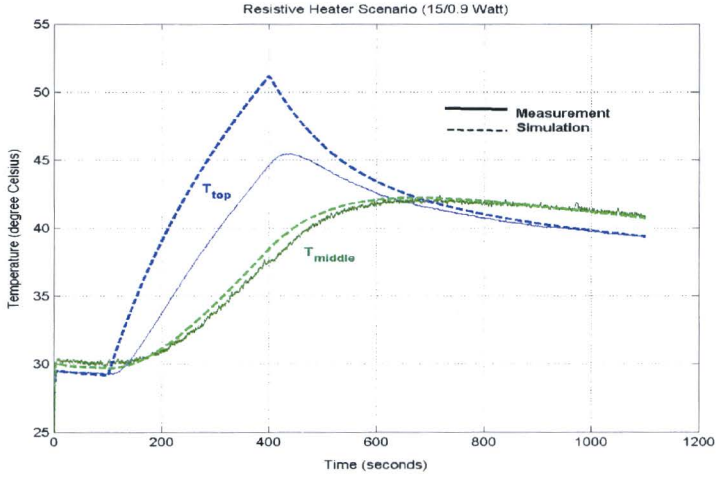

Figure 31.
Resistive Heater Scenario

The heating scenario started at t=100 seconds. Remaining characteristics were kept to their standard values as discussed in previous chapters. Evaluating the data of Figure 31 and especially comparing them with the results depicted in Figure 18b, support the assumption that the theoretical considerations are being confirmed by the experimental practice: The rounding off of the temperature curves (especially 'T_{top}') is also visible between 3D and 1D models in Figure 18b in consequence of the increase in geometric and functional detail from 1D to 3D modeling.

Combined RH&PE Scenario

In this experiment the RH and PE were applied simultaneously. For the RH the same scenario was used as in the previous test while for the PE a setting was chosen of 7.0/-2.5 Watt. Switching point was set at t=400 seconds after a 300 seconds heating up, the same timing as in the previous experiment with only

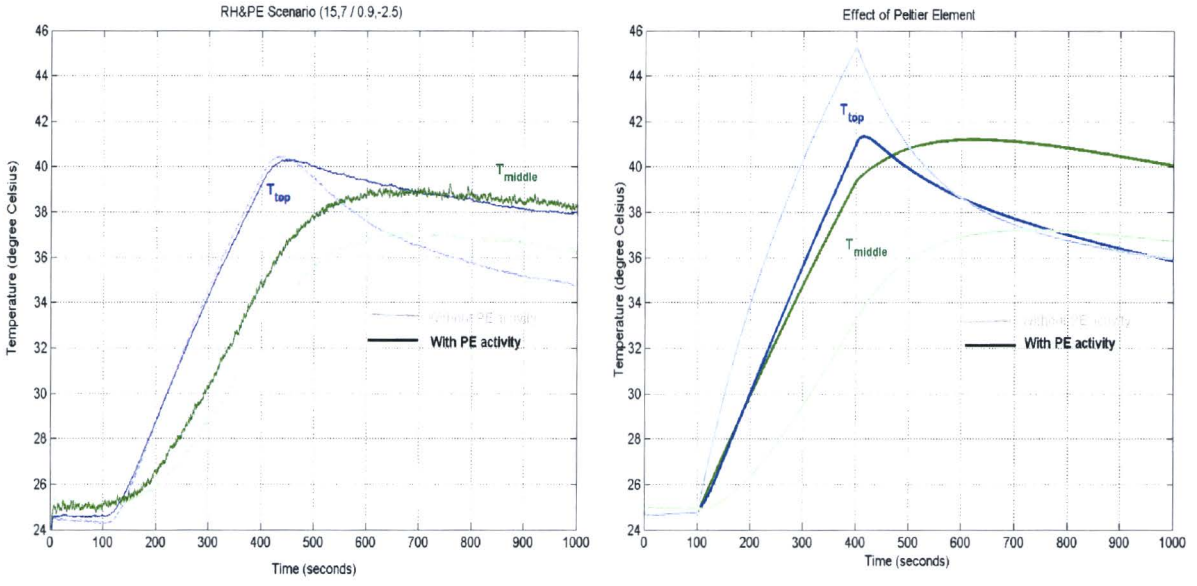

a)Experiments *b)Simulations*

Figure 32
Combined RH&PE Scenario

the RH active. In Figure 32a the experimental results are shown with the previous RH scenario as reference with its temperature data shifted 5°C down for better comparison. Contrary to what was expected (see simulation in Figure 32b) there is obviously only limited heat transport through the Peltier Element downwards to the cuvet area at the cost of heat flow upwards to the top area of the incubator. Similar to the situation with the PE experiment as presented in Figure 30, a simulation was performed under the assumption of a significantly increased internal heat conductance for the PE. Again the model results agree considerably better with the actual observed experimental results as depicted in Figure 33. Although the possible malfunctioning of the PE exhibits a certain consistency further inquiries are

necessary before any conclusive statement can be made.

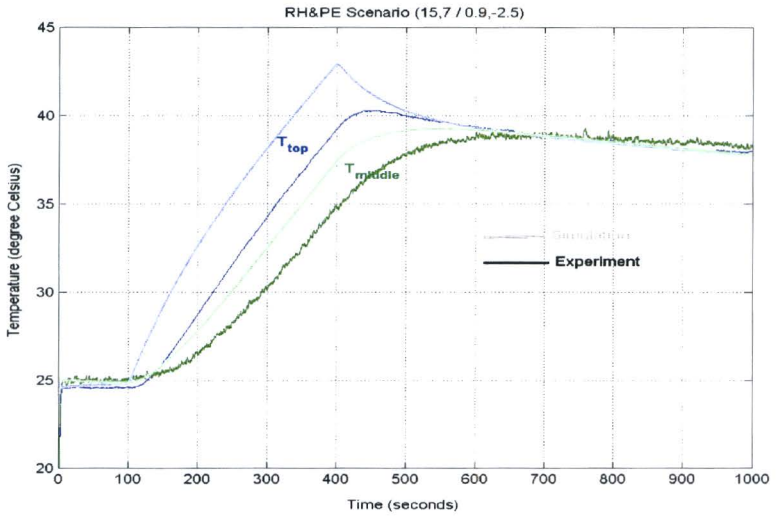

Figure 33
Combined RH&PE Scenario experiment.
Simulation with PE characteristics adjusted as reference.

Regulation

In paragraph IV3 the regulation of the temperature and the temperature-gradient was discussed. The

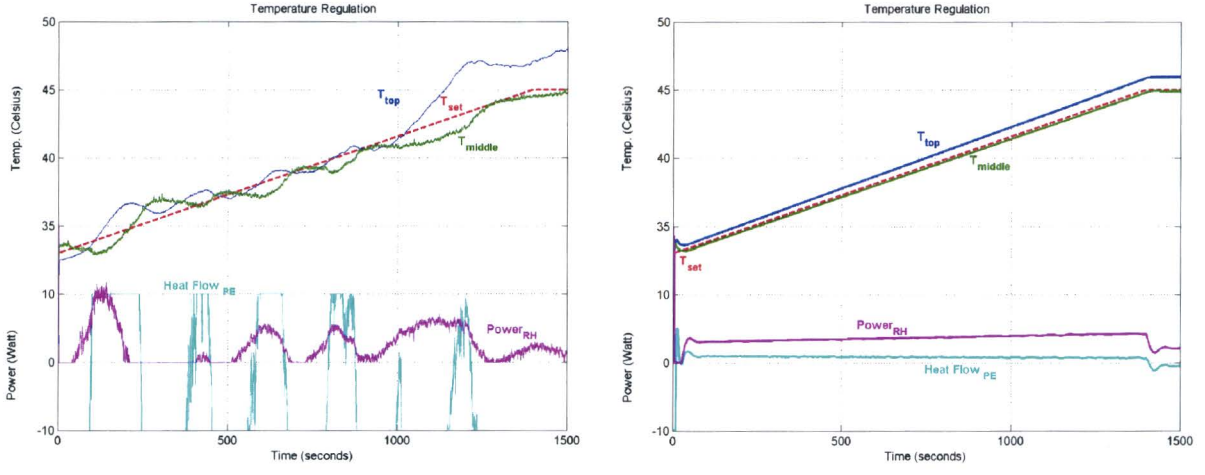

Figure 34
Temperature and Temperature-Gradient Control, Experimental Setup(left) and Model (right).

experimental verification is depicted in Figure 34 (left) and once more the outcome deviates considerably from the theoretical expected results (right). Adjustment of the PE characteristics in the model in the

same way as before caused again a shift of the model results towards the actual observed situation as depicted in Figure 35.

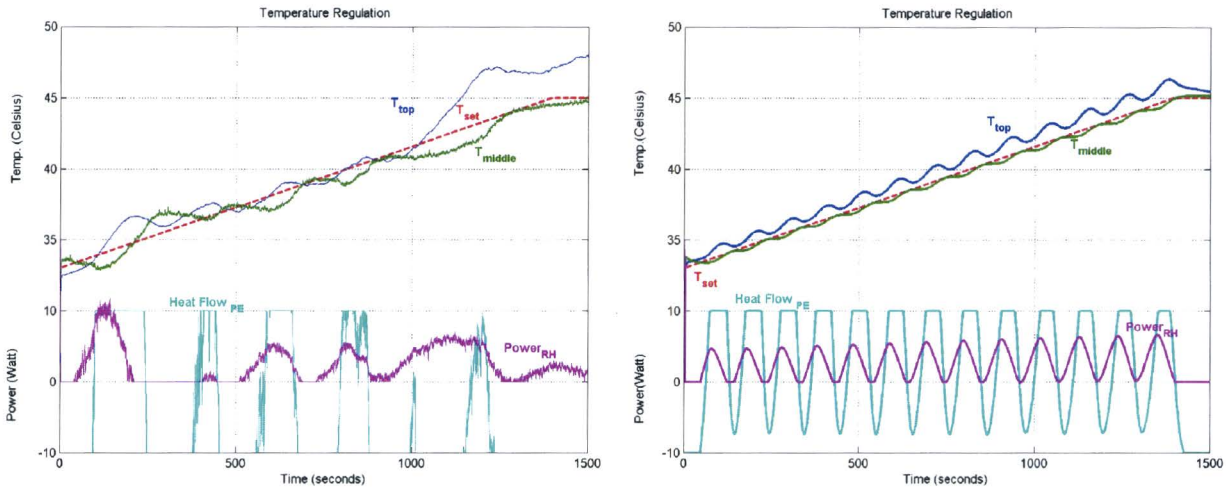

Figure 35
Temperature and Temperature-Gradient Control, Experimental Setup(left) and Adjusted Model (right).

Peltier Element Malfunctioning

The experimental results as described and analyzed above suggest a malfunction of the PE. Driver and sensing electronics were examined and proved correct.

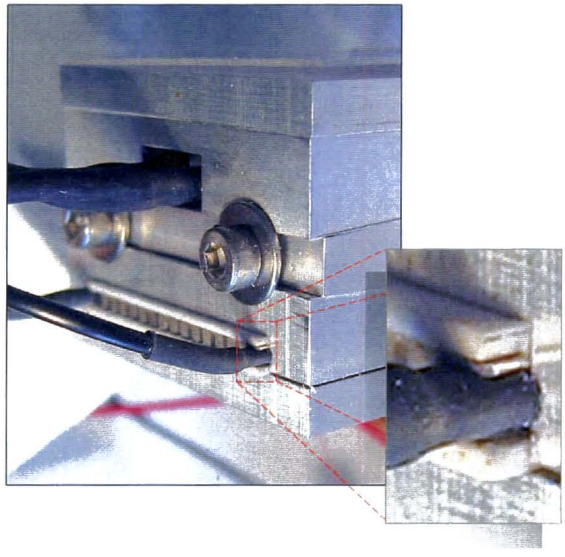

Figure 36
Incubator details.

A deeper look into the incubator body however reveals a possible cause for the problems. The layout of

the incubator is given in Figure 9 and a detailed photograph of its actual realization is shown in Figure 36. This picture gives a detailed view on the power block of the incubator with the clearly visible PE. Instead of being sandwiched between 2 sheets of aluminum the PE is tightly mounted in a u-shaped block. Although special care is taken that this block does not make direct thermal contact with the aluminum sheet underneath the PE it nevertheless looks as if no precaution is taken to avoid the legs of the u-shape from thermally short-circuiting the top and bottom of the PE.

VI CONCLUSIONS

The considerations with respect to sample evaporation and direct sight on the 3D-MicroArray during hybridization led to the basic concept of a gradient incubator. Choices for geometries, components and materials were made and used for a 3D-Finite Element-model. Computations supported previous assumptions regarding the formation of cold spots in the glass cover over the sample cuvets and confirmed the feasibility of the gradient concept as well. It was also ascertained that time constant effects emanating from the use of an extra heat resistance introduced to create the desired temperature gradient could be addressed effectively by also incorporating the foreseen heat pump in the control system.

Next a 1D dynamic system model was conceived that enabled a simplified description of the timely behavior of the 3D-MicroArray incubator. This model was compared with the 3D computational model and it was proved that both were in agreement. It could be concluded that independent separate control systems for temperature and temperature-gradient would optimally regulate the incubator. Such regulators were implemented in the 1D dynamic system model of the incubator and proved to function in the simulations as expected.

Finally the gradient concept is experimentally tested. Incubator hardware, driver and sensor electronics and computer interface with supporting software were realized and as far as possible tested modularly. Total system measurements were performed and compared with equivalent model computations. From these measurements it can be concluded that the thermal behavior of the 3D-MicroArray incubator was mainly in accordance with the heat circuit as described and modeled. Heat capacitances, resistances and resulting time constants were clearly recognizable and did agree with the theoretically derived values.

The RH produced thermal power and did heat up the incubator as expected. On the contrary the PE did not perform as specified. The measured temperature gradient was over 5 times smaller than computed whereas the collateral heat produced by the PE did agree. The hypothesis of a kind of thermal short-circuit of the PE by the incubator construction was brought up and used to compare results in such a situation with model calculations. The assumption proved realistic and was further supported by close examinations of the respective region of the incubator.

The impossibility to generate adequate circulating heat flow and thus to control the gradient incubator, prevented the ultimate proof of its concept. The experiments however also indicated that the heat pump problem is the only stand in between towards this proof.

I THE POLYMERASE CHAIN REACTION (PCR)

1 Introduction

The PCR technique was invented in 1985 by Kary B. Mullis[5] while working as a chemist at the Cetus Corporation, a biotechnology firm in Emeryville, California, USA. Nowadays, thanks to this technique, scientists are capable of making millions of copies of a specific part of even a single DNA molecule. This revolutionized many aspects of current research such as the diagnosis of genetic defects or the monitoring of and subsequent intervention in the treatment of AIDS. In recent years the technique is also being used by criminologists to link specific persons to minimal traces of human origin via DNA comparison.

2 PCR Technology

The polymerase chain reaction is a test tube system for DNA replication that allows a "target" DNA sequence to be selectively amplified, or enriched, several million-fold in just a few hours. Within a dividing cell, DNA replication involves a series of enzyme-mediated reactions, whose end result is a faithful copy of the entire genome. Within a test tube, PCR uses just one indispensable enzyme - DNA polymerase - to amplify a specific fraction of the genome.

In the cellular situation (when replicating DNA) enzymes first unwind and denature the DNA double helix into single strands [4]. Then, RNA polymerase synthesizes a short stretch of RNA complementary to one of the DNA strands at the start site of replication. This DNA/RNA heteroduplex acts as a "priming site" for the attachment of the DNA polymerase, which then produces the complementary DNA strand. During PCR (Figure 37) high temperature is used to separate the DNA molecules into single strands, and synthetic sequences of single-stranded DNA (20-30 nucleotides) serve as primers. Two different primer sequences are used to bracket the target region to be amplified. One primer is complementary to one DNA strand at the beginning of the target region; a second primer is complementary to a sequence on the opposite DNA strand at the end of the target region. To perform a PCR reaction, a small quantity of the target DNA is added to a test tube with a buffered solution containing DNA polymerase, the two specific oligonucleotide primers and the four deoxynucleotide building blocks of DNA. The PCR mixture

[5] The invention of PCR was not the result of targeted research. Mullis conceived the idea while cruising in a Honda Civic on Highway 128 in California. He received a bonus of $10,000.- from Cetus. Later Cetus sold the technology to LaRoche for $300,000,000,-. Mullis won the Nobel Prize in Chemistry in 1993.

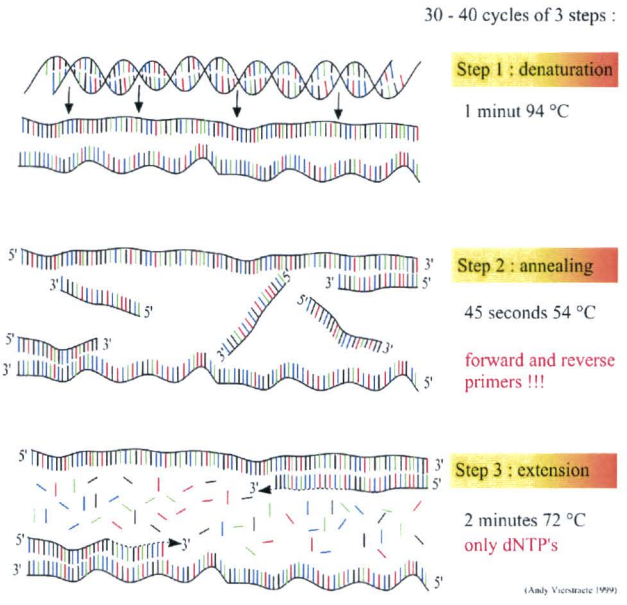

Figure 37
Polymerase Chain Reaction, adapted from [5]

is taken through replication cycles consisting of:

- one to several minutes at 94-96 °C, during which the DNA is denatured into single strands,
- one to several minutes at 50-65 °C, during which the primers hybridize or "anneal" (by way of hydrogen bonds) to their complementary sequences on either side of the target sequence, and
- one to several minutes at 72 °C, during which the polymerase binds and extends a complementary DNA strand from each primer.

As amplification proceeds, the DNA sequence between the primers doubles after each cycle. Following thirty such cycles, a theoretical amplification factor of one billion is obtained.

II MICROARRAY TECHNOLOGY AND COMBINATORIAL CHEMISTRY[6]

1 Introduction

In the late 1980s, a team of scientists led by Stephen P.A. Fodor, PhD. [6] enabled breakthroughs in genome research by inventing and further developing micro array technology. They had the insight to combine semiconductor manufacturing techniques with advances in combinatorial chemistry. In this way they realized a well defined pattern of cells on a substrate with per cell identical single stranded DNA-molecules running into a connection to the surface.

At the same time the human and other important genomes were being sequenced and made available through public databases such as the one created by the Human Genome Project. The combination of knowledge of the genetic sequence of an organism with the powerful possibilities of the micro array chip technology changed the study of modern biology

2 Combinatorial Chemistry and Chip Technology

In Figure 38 on the left a schematically representation is given of the selective addition of specific nucleotides to surface bounded DNA-fragments. These DNA-fragments (arranged in matrix cells on a semiconductor wafer) are per cell masked or released for reaction with the nucleotide momentarily in solution. As there are four different types of nucleotides this process has to be repeated maximally four times before all DNA-fragments on the chip have been extended with one specific nucleotide.

In Figure 38 on the right the micro array resulting from one hundred cycles as described above is depicted. Every cell contains cell-specific DNA-fragments of twenty five nucleotides. These DNA-fragments are single stranded and stand open for eventually binding with their complementary counterparts. Thanks to modern production technologies, stemming from the micro-electronics industry, chips with up to 500,000 cells are possible.

[6] Images courtesy of **Affymetrix**

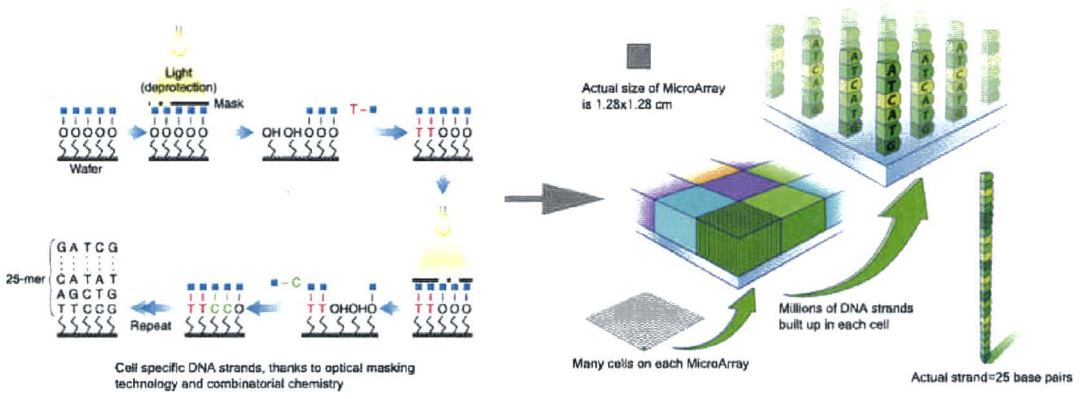

Figure 38
Schematics of the production of a micro array

The application of a micro array is shown in Figure 39. The composition of a mixture of DNA- or RNA-fragments resulting from a PCR-like process with nucleotides comprising fluorescent labels becomes clear after reacting with an appropriate micro array. Where complementary RNA/DNA molecules hybridize, fluorescence will be detected, indirectly yielding the identity of these molecules.

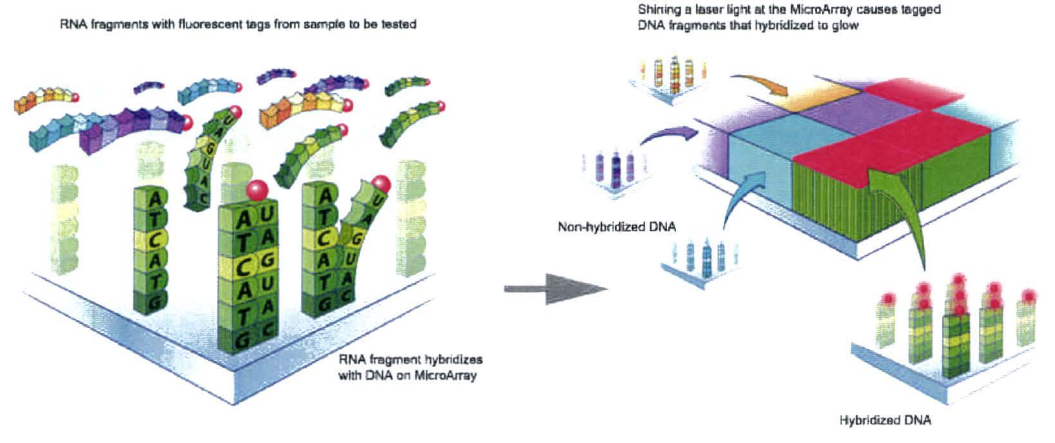

Figure 39
Detection of specific RNA-sequences with a Micro Array

This way researchers can broadly address the genome at once and not just a few genes at a time with experiments lasting hours instead of weeks or even more.

Figure 40 shows a resulting picture after laser scanning. Intensity, color and position represent the wanted information for every individual cell.

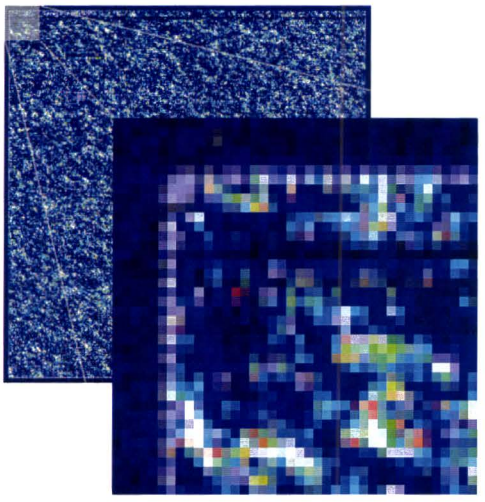

Figure 40
Reading of a Micro Array chip after incubation

Yet there are some drawbacks with respect to the first arisen Micro Array Technology as described above:

First of all the development of lithographic masks requires a long lead time. Also costs are considerable whereas the vast amount of reactions that can be addressed simultaneously is not always required.

Secondly, however large the number of micro array cells acting simultaneously on the same sample, the reactions in every single one of them are rather slow. Diffusion limitation experienced by the relatively large DNA/RNA molecules in the mostly 2D-geometry of the system reduces the hybridization rate between counterparts in a specific cell. This results in overall sample incubation times of up to 24 hours.

As a low cost alternative the research community came up with the microscope glass slide variant in substitution for the lithographic microchip. In this approach very small amounts of reagent are dispensed on a microscope slide with highly accurate equipment based on inkjet technology, every droplet containing a different reagent, in fact short single stranded DNA fragments alike the ones constructed in every cell of the lithographic micro array. These DNA molecules and the glass slide are prepared in such a way that the strands become attached to the surface, again much alike the strands in a cell in the lithographic micro array. So up to a few thousands spots can be created on a microscope slide and incubation with a sample resulting from a PCR reaction will give comparable results as with a lithographic micro array. (See Figure 41)

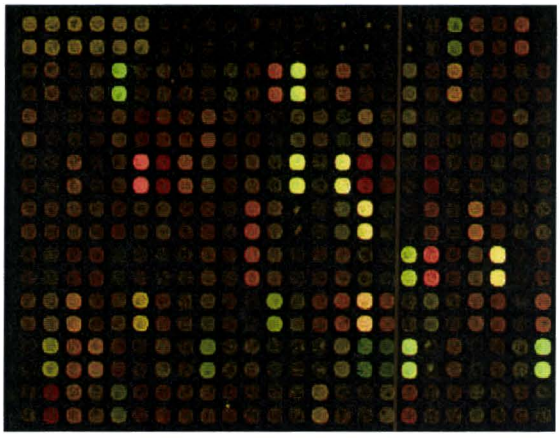

Figure 41
Microscope slide micro array

Although these microscope slide micro arrays are economically preferable and much more flexible than their lithographic equivalents, they certainly exhibit the same long incubation times.

III 3D-MICROARRAY INCUBATOR MODEL IN FEMLAB® 3.0

1 Introduction

In chapter III paragraph 1&2 the layout and material characteristics of the 3D-MicroArray Incubator underlying its Femlab® model have been presented and discussed. Results have been shown and supported the starting points used for the basic design of this incubator.

In this chapter some more details with respect to this model will pass in revue leading to a statement on model reliability and application restrictions.

2 Physical aspects

Equation (3) is the standard heat transport equation that is being solved by the software when evaluating this incubator model. The settings for ρ, c_p , q and κ have been discussed in detail in chapter III. The boundary condition (4) needs further consideration. As mentioned before; all outside

$$\rho \cdot c_p \cdot \frac{\partial T}{\partial t} - \nabla \bullet (\kappa \nabla T) = q \qquad (3)$$

$$\vec{n} \bullet (\kappa \nabla T) = q_o + h(T_\infty - T) + const.(T_{amb}{}^4 - T^4) \qquad (4)$$

surfaces of the incubator are considered fully insulated with exception of the top surface. This means that for this top surface the right hand side of (4) is different from zero and has to be taken into account follows:

1. As there is no heat source active: $q_0 \equiv 0$.
2. Both natural convection and radiation significantly contribute to the heat loss via the top surface. As the relevant temperature differences are maximal in the range of 50 °C *'Newton's law of cooling'* holds. This law states that the rate of cooling of a hot body which is loosing heat, both by radiation and by natural convection, is proportional to the difference in temperature between it and its surrounding as long as no large temperature excesses are involved. This means that with an adequate setting of the *'heat transfer coefficient': h,* both phenomena can be dealt with and the radiation term can be switched off by putting *'const.=0'.* Consequently the magnitude of the *heat transfer coefficient h* in the situation of the incubator is determined by these 2 phenomena. The radiation part adds 5 $\leftrightarrow$ 10 W/m^{2}K [7] to *h* and natural convection in turn adds 5 $\leftrightarrow$ 15 W/m^{2}K [8] . Simulations have been performed with settings for *h* of 10 and

25 W/m^{2}K.

It needs special attention to compose a heat circuit that consists of piled sheets of material (as the 3D-MicroArray Incubator does) because every transition between adjacent sheets will create an extra thermal resistance in the heat circuit. This may significantly influence the working of the incubator and make overall results unreliable. In Figure 42 and Figure 43 the two most likely situations with respect to the above are depicted.

1. Figure 42a shows a situation where the sheets are bent often in consequence of a wrong construction leaving a void over the larger part of the foreseen contact area. Assuming a mean of 0.1 mm for the height of the slit it can be concluded that heat transport between both sheets through the enclosed air layer only takes place via conduction. If e.g. there is such a layer between the PVC heat resistor sheet and the aluminum top sheet above it (see Figure 9d and Figure 9e than an extra heat resistance will be introduced in the heat flow circuit

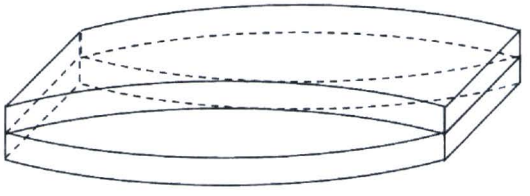

a) Slit formation

Heat flow through a pile of 2 sheets (Al, 2mm each) with an air slit in between (80%,x0.1mm). ΔT=10°C. b)

Figure 42
Heat circuit construction pitfalls

with a conductance of 0.349 W/K (κ_{air}=0.026 W/mK) [3] which is of the same order of magnitude as the PVC heat resistor itself (0.215 W/K see Table 2). Model results would certainly be influenced as the example in Figure 42b demonstrates. So special care has been taken to avoid this kind of slits and as shown in paragraph V1 the construction of the 3D-MicroArray Incubator is such that mechanical torsion causing the bending of the individual sheets will be minimal and well controlled.

2. Another possible cause of deteriorated thermal contact is schematically depicted in Figure 43. Here surface roughness hinders the full contact of two further flat sheets of material. A simple

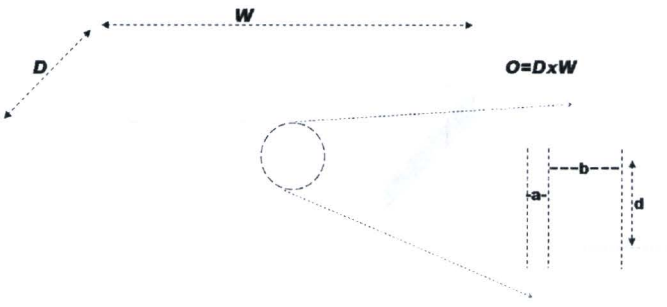

Figure 43

estimation shows that in a situation as shown in the detailed picture of Figure 43 we can write for the thermal conductance of the slit area (κ is specific conductance of the sheet with the rough surface):

$$K_{slit} = \frac{\kappa \cdot O}{d} \cdot \frac{a}{b} \qquad (5)$$

This means that in case of a flat PVC surface pressed on a rough aluminum one with $d = 0.1\,mm$ and $a = 0.01b$ (*i.e. only 1% direct surface area contact*) the specific conductance decreases by a factor of $b/a \approx 100$. However even if the thermal contact between the aluminum top and the PVC sheet in the 3D-MicroArray Incubator would be of this quality the thermal resistance of the slit area would be 200 fold smaller than that of the PVC sheet and consequently negligible.

3 Mathematical aspects

After accepting the 3D-model of the MicroArray Incubator as represented in Chapter III as an adequate conception of its physical realization as described in paragraph V1 the correctness of the computation of its physical behavior as performed by the Femlab® software has to be discussed. Because direct proof of this is not possible within the scope of this work, circumstantial evidence will be presented to support the claim.

1. In paragraph IV2 another dynamic system model for the 3D-MicroArray Incubator has been presented. In Figure 18 results of this model are compared with computations performed with the Femlab® model each time for identical scenarios of power setting and top surface cooling. Three such comparisons took place. As already stated there the results of both models are in full accordance with each other and thus also highly supportive for the correctness of the Femlab® numerical algorithms.

2. Because of some small dimensions in the model like the thin (0.5mm) glass cover the meshing of the 3D model in Femlab® resulted in over 188,000 elements (see Figure 44a). A more coarse setting of the meshing was not possible with the software and a finer setting met with

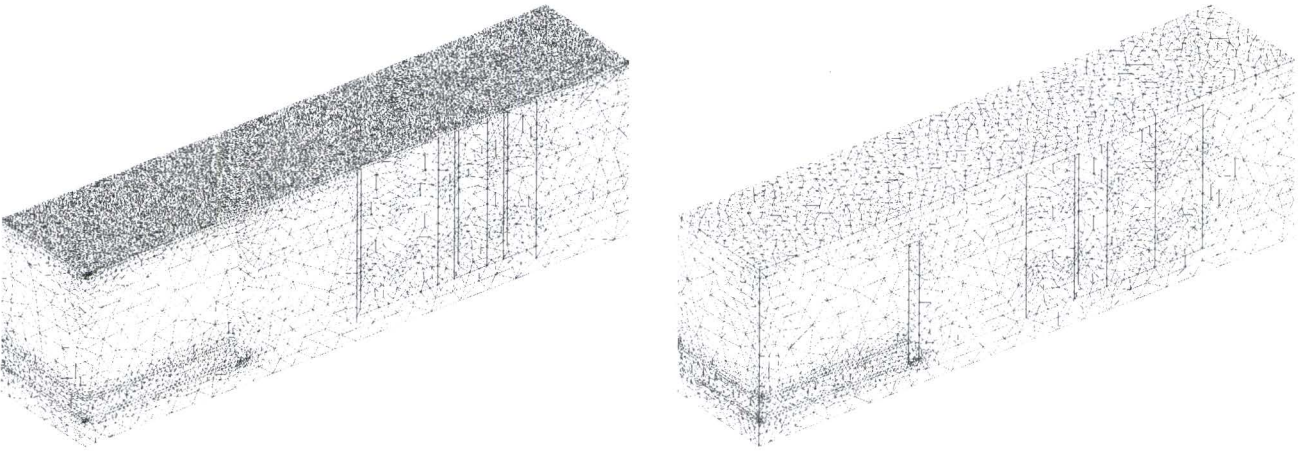

a) Glass cover 0.5 mm. 188,000 elements

b) Glass cover 1.5 mm. 101,000 elements

Figure 44
Femlab meshing (coarse).

computer restrictions thus making this kind of accuracy evaluation impossible. By slightly changing the model it was possible to get around this problem. After increasing the thickness of the glass cover to 1.5 mm the number of meshes went down to just over 101,000 elements as shown in Figure 44b. Pictures in Figure 45 (corresponding with Figure 44) give the results after running both models with identical scenarios. Both results are displayed with the same temperature scale covering a range 66→75°C and show much similarity. Only in two aspects significant disparity can be noticed.

First of all it is clear that with the 0.5 mm glass cover the overall temperature of the incubator is ca 1.3°C higher than with the 1.5 mm one. This difference however can be fully explained by the fact that the total heat capacity of the incubator because of this extra millimeter of glass increases from 254 to 262 J/K and is responsible for a 3% lower temperature increase at the same total heating power. This comes down to a 1.4°C smaller temperature rise in this situation and is in accordance with the simulation results.

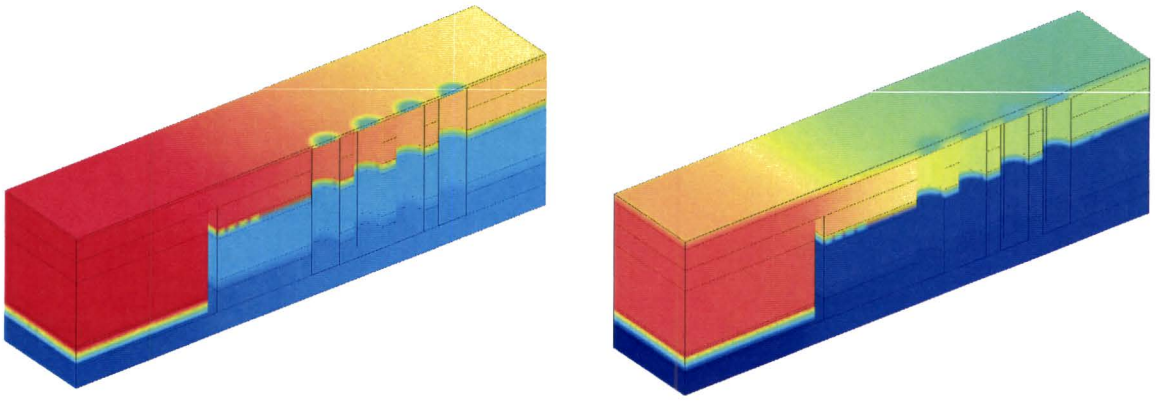

a) Glass cover 0.5 mm.

b) Glass cover 1.5 mm

Figure 45
Influence of increasing thickness of glass cover.

The second aspect that needs consideration is the less pronounced temperature dent over the cuvet area in the 1.5 mm glass cover. This stems mainly from the fact that heat loss via the top is more or less the same for the 1.5 mm glass cover as it is for the 0.5 mm one because much the same heat flow has to be supplied in both situations somewhat horizontally through the glass over the cuvet void to replenish this heat loss. Therefore in first approximation the temperature gradient will be three times less because of the three times thicker glass cover thus causing a three times smaller temperature dent.

3. Further support for the reliability of the computations is shown in Figure 46. Here the temperature time curve is shown for the three locations corresponding to Figure 13c. It concerns four simulations; one with a glass cover of 0.5 mm, the rest with a 1.5 mm one but with three different mesh settings (101,000 128,000 and 156,000 elements). From the graphs it is clear that different mesh settings do not change the results significantly. The differences between the 0.5 mm computation on the one hand and the 1.5 mm ones on the other have been elucidated above.

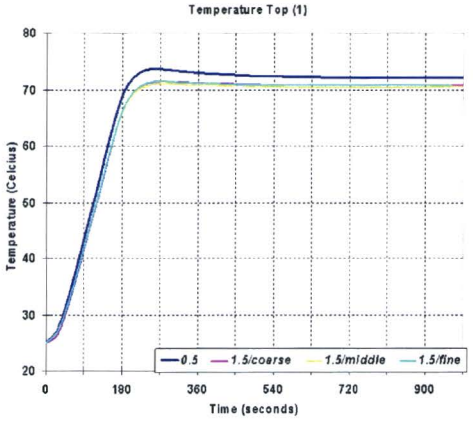

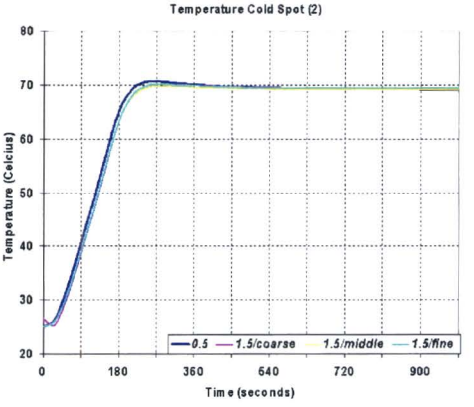

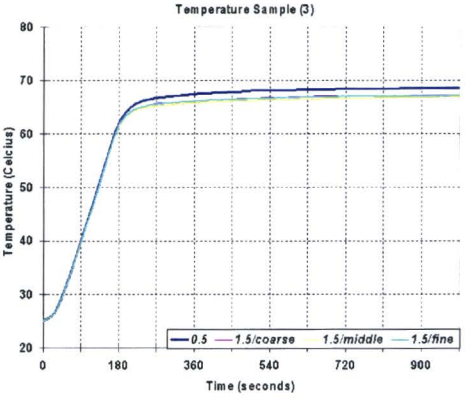

Figure 46
Temperature diagrams for 3 positions in 4 simulations.

Conclusive proof for the reliability of the Femlab® computations could not be given. Yet the circumstantial evidence as represented here is such that it seems fully acceptable to act as if.

IV 3D-MICROARRAY DYNAMIC SYSTEM MODEL IN SIMULINK®

In chapter IV the physical aspects of the 3D-MicroArray Incubator have been put in perspective. This resulted in a rather simple dynamic model that showed an excellent conformity with the behavior of the 3D-Femlab® model. In this chapter the detailed description for the Simulink® model of this dynamic system is given.

In Figure 47 the top layer of the dynamic system model is shown. The colored block encompasses the functionality of the incubator and its supporting hardware. The other bocks are foreseen for control and data -logging and -display.

The 'Temp.Setting'-block (in detail below) delivers the desired temperature trajectory which signal is compared with the actual temperatures. In this way 2 signals are derived; one representative for the deviation of the actual temperature from the desired one and another signal representative for the temperature gradient in the system. These signals are fed into the 'Regulator'-block where the optimal settings for the RH and the PE are computed.

Signals running during a simulation are real time shown via the 2 display-blocks and/or stored in a disk file via the 'Out1'-terminal.

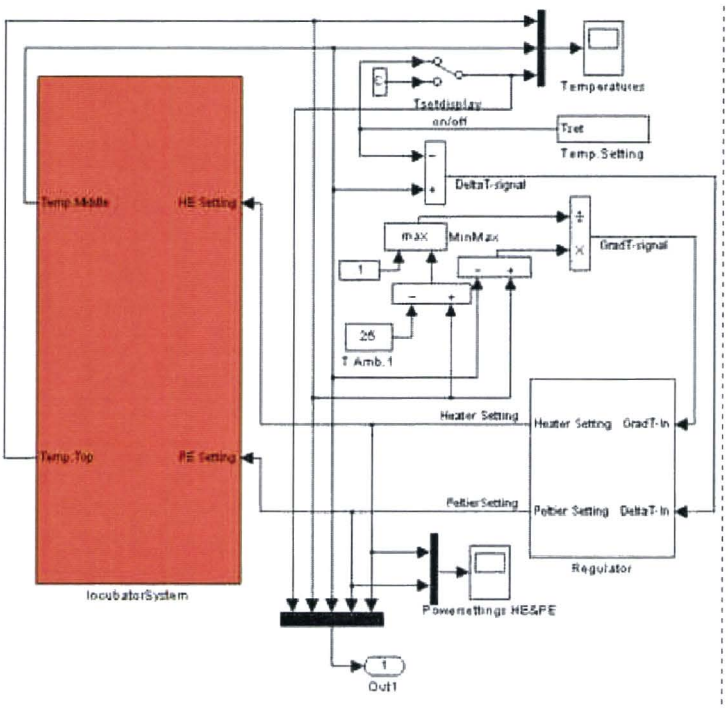

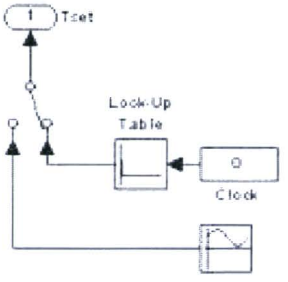

Temperature Setting

Figure 47
Top-layer Dynamic System Model

In Figure 48 the 'Regulator'-block and its sub-blocks are presented in detail.

At the top of Figure 48 the layout of the 'Regulator'-block is shown. Here the 'PID-regulator', depicted in the middle of Figure 48, consists of 2 PID controllers; one computing the power setting for the Resistive Heater, the other computing the circulating power to be generated by the Peltier Element. Both controllers are used in the proportional mode only.

At the bottom of Figure 48 the 'Open Loop'-block is shown. This block offers some means to define power scenarios for specific test purposes.

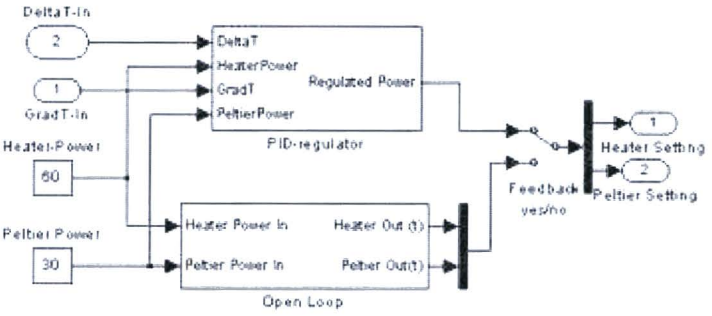

Regulator

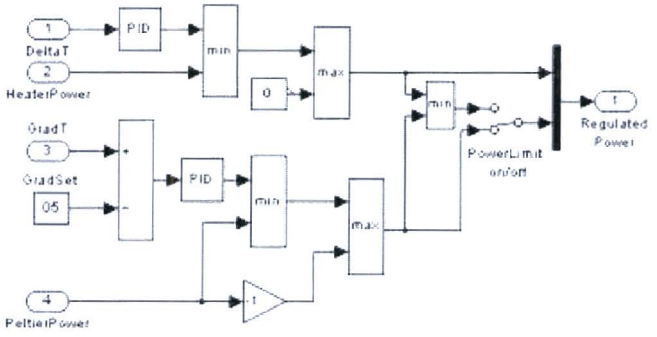

PID-Regulator

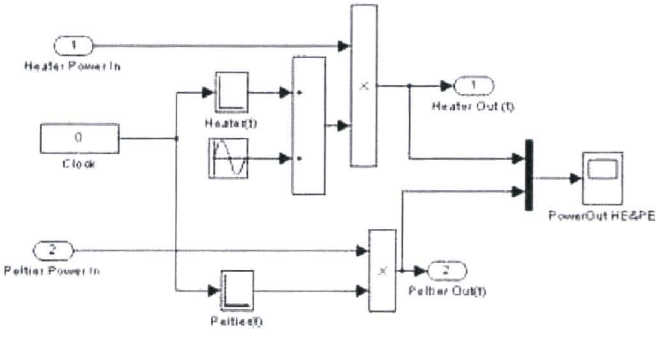

Open Loop

Figure 48
Regulator Dynamic System Model

The dynamic model in the IncubatorSystem-block consists of two major parts; the Incubator-Body and the Heater&Peltier-Element. See Figure 49 (top right). Both blocks are embedded between real time display blocks and variables allowing initial settings when simulating.

Inside the IncubatorBody-block (Figure 49, bottom right) three heat capacitors are situated ('Top', 'Middle' and 'Bottom'). Each heat capacitor block (e.g. Figure 49, bottom left) divides the input (heat flow) signal by a number equal to the magnitude of the concerning heat capacitor and integrates this signal over time. The result is the desired heat capacitor (temperature) signal.

The input (heat flow) signal to each heat capacitor is computed on the principle that heat flow between adjacent heat capacitors equals the difference between the (temperature) signals on these capacitors multiplied by the magnitude of the heat conductance between them.

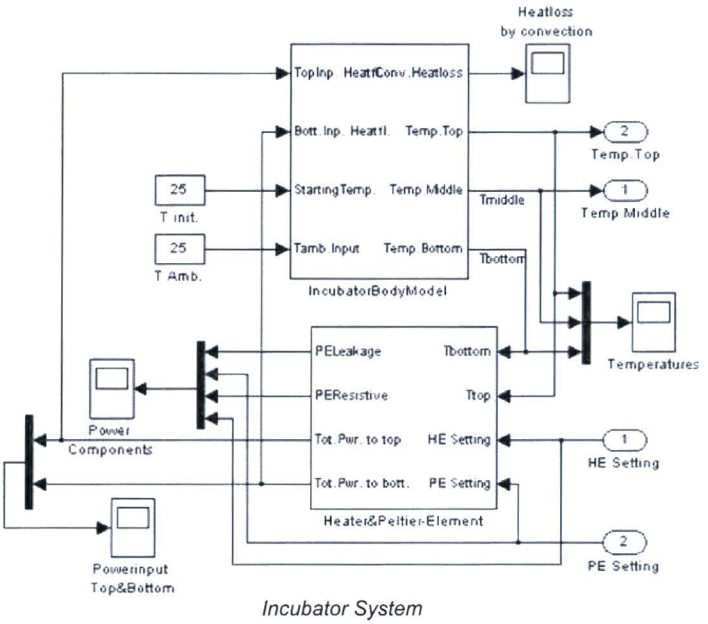

Incubator System

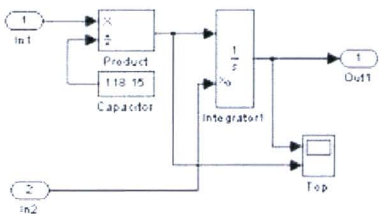

Top (Heat Capacitor)

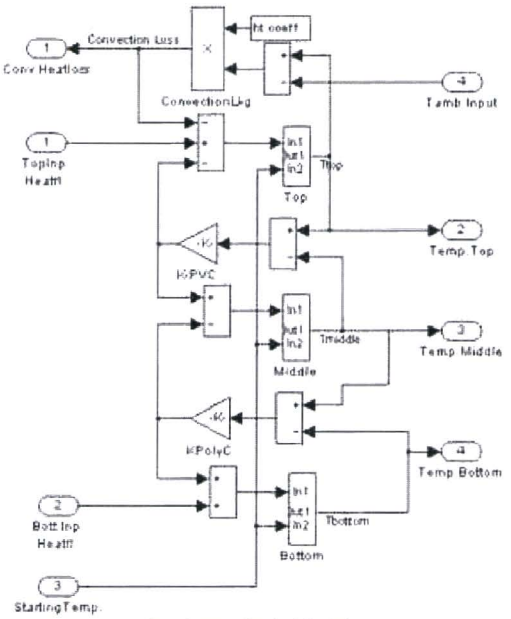

Incubator Body Model

Figure 49
Incubator System Model

The layout of the Heater&Peltier-Element block is given in Figure 50. In the top-right of this figure the several power sources are inputted and combined to the top- and bottom- heat flows that enter the incubator body (see Figure 16).

The 'Peltier Element' block (see 'bottom-right') computes for the regarding element the resulting electrical current and the heat power that goes with it on the basis of the 'PE circulating heat flow'-setting.

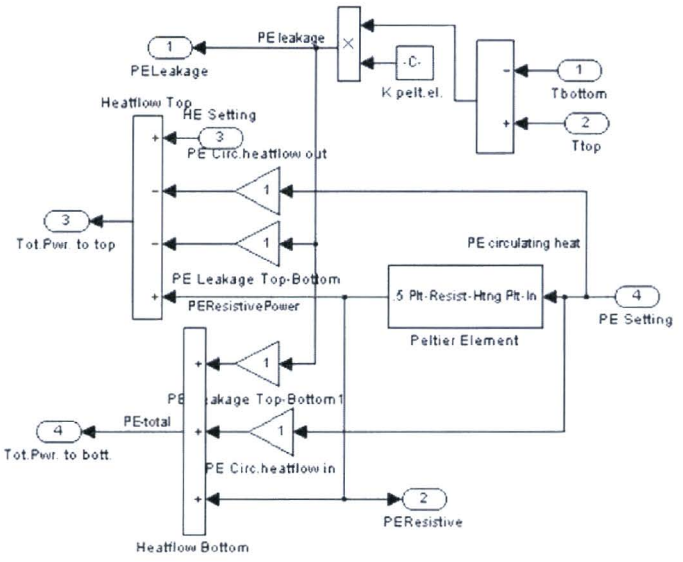

Heater&Peltier-Element

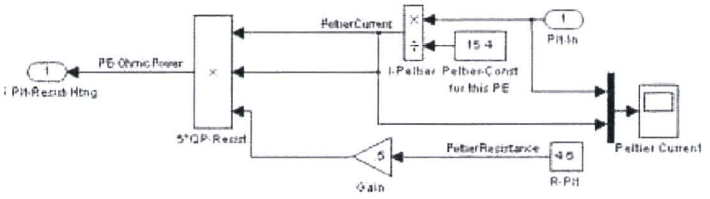

Peltier Element

Figure 50
Heater and Peltier Element

The dynamic model for the situation where instead of the 'IncubatorSystem' block the 'TUeDACS/1 QAD Interface' block is incorporated (see Figure 24 right) is, apart from that aspect, identical.

The simulations have been run with an ode2 (Heun) solver in Simulink®4 in combination with Matlab®6.1. To guarantee the correct working of the TUeDACS/1 QAD interface a fixed step size was chosen for the solver. Computations were done with a step size of 0.1 second. As a control several computations were repeated with a 10-fold step size of 1 second. No differences, relevant for the application, were noticed.

1 References

1] **H. van Damme**, Organon Teknika Netherlands: *Personal communication, 1999*

2] **W.Mathias Howell, Magnus Jobs, Anthony Brookes.** Center for Genomics and Bioinformatics, Karolinska Institute, S-17177, Stockholm: *An Improved Fluorescence System for DNA Melting Analysis.*

3] **L.P.B.M. Janssen, M.M.C.G. Warmoeskerken,** Delftse Universitaire Pers ISBN 90 407 1.302 2: *Transport Phenomena Data Companion.*

4] http://highered.mcgraw-hill.com/sites/0072437316/student_view0/ chapter 14, animations

5] **Andy Vierstraete,** http://allserv.ugent.be/~avierstr/ .

6] **S.P.A. Fodor, J. Read, M. Pirrung, L. Stryer, A. Lu, D. Solas,** Science 251 (4995), 767-73, 1991: *Light-directed, spatially addressable parallel chemical synthesis.* (This landmark publication was the first reported description of microarray technology. It also first described combinatorial chemistry techniques for generation of large chemical libraries).

7] **H.E.A. van den Akker, R.F. Mudde,** Delft University Press,:*Fysische transportverschijnselen 1,* page 155.

8] Elsevier, 49^{e} druk,: *Poly Technisch Zakboek,* page **E1**/17